NAVAL POSTGRADUATE SCHOOL
Monterey, California

THESIS

MEASUREMENTS WITH WIRE MESH STACKS IN THERMOACOUSTIC PRIME MOVERS

by

Mark S. Reed

June, 1996

Thesis Advisor:	Thomas J. Hofler
Co-Advisor:	Anthony A. Atchley

Approved for public release; distribution is unlimited.

REPORT DOCUMENTATION PAGE

Form Approved OMB No. 0704-0188

1. AGENCY USE ONLY *(Leave blank)*	2. REPORT DATE June 1996	3. REPORT TYPE AND DATES COVERED Master's Thesis

4. MEASUREMENTS WITH WIRE MESH STACKS IN THERMOACOUSTIC PRIME MOVERS	5. FUNDING NUMBERS N0001496WR20003
6. AUTHOR(S) Mark S. Reed	
7. PERFORMING ORGANIZATION NAME(S) AND ADDRESS(ES) Naval Postgraduate School Monterey CA 93943-5000	8. PERFORMING ORGANIZATION REPORT NUMBER
9. SPONSORING/MONITORING AGENCY NAME(S) AND ADDRESS(ES) Office of Naval Research	10. SPONSORING/MONITORING AGENCY REPORT NUMBER

11. SUPPLEMENTARY NOTES The views expressed in this thesis are those of the author and do not reflect the official policy or position of the Department of Defense or the U.S. Government.

12a. DISTRIBUTION/AVAILABILITY STATEMENT Approved for public release; distribution is unlimited.	12b. DISTRIBUTION CODE

13. ABSTRACT *(maximum 200 words)*

This thesis documents the first measurements of a thermoacoustic prime mover using wire mesh screens as the stack material. A thermoacoustic prime mover is a heat engine which converts thermal energy to sound. The stack material is sandwiched between the hot and cold heat exchanger and exchanges heat with the cycling gas elements flowing in the stack. The experimental stacks were constructed by inserting disks cut from wire mesh in a tube. In addition to simplicity, these stacks have two significant advantages. First, the wire is relatively impervious to moderately high temperatures and second, the effective thermal conductance of the structure is one to two orders of magnitude lower than a comparable metal "parallel plate" structure. Since no linear theoretical thermoacoustic models exist for these wire mesh stacks, the approach taken was simply to measure the performance of several different mesh stacks. Results gathered from two different prime movers indicate acoustic onset temperatures and amplitude performance comparable to the best data for parallel plate stacks. Moreover, measured efficiencies for mesh stacks appear to be substantially higher than for parallel plates.

14. SUBJECT TERMS Acoustics; Thermoacoustics; Thermoacoustic Prime Mover; Thermoacoustics Prime Mover Stack			15. NUMBER OF PAGES 71
			16. PRICE CODE
17. SECURITY CLASSIFICATION OF REPORT Unclassified	18. SECURITY CLASSIFICATION OF THIS PAGE Unclassified	19. SECURITY CLASSIFICATION OF ABSTRACT Unclassified	20. LIMITATION OF ABSTRACT UL

NSN 7540-01-280-5500

Standard Form 298 (Rev. 2-89)
Prescribed by ANSI Std. 239-18 298-102

Approved for public release; distribution is unlimited.

MEASUREMENTS WITH WIRE MESH STACKS IN THERMOACOUSTIC PRIME MOVERS

Mark S. Reed
Lieutenant Commander, United States Navy
B.A., Shippensburg State College, 1982

Submitted in partial fulfillment
of the requirements for the degree of

MASTER OF SCIENCE IN APPLIED PHYSICS
from the

NAVAL POSTGRADUATE SCHOOL
JUNE 1996

Author: Mark Stephen Reed

Mark S. Reed

Approved by: Thomas J. Hofler

Thomas J. Hofler, Thesis Advisor

Anthony A. Atchley

Anthony A. Atchley, Thesis Co-Advisor

W. B. Colson

William B. Colson, Chairman
Department of Physics

ABSTRACT

This thesis documents the first measurements of a thermoacoustic prime mover using wire mesh screens as the stack material. A thermoacoustic prime mover is a heat engine which converts thermal energy to sound. The stack material is sandwiched between the hot and cold heat exchanger and exchanges heat with the cycling gas elements flowing in the stack. The experimental stacks were constructed by inserting disks cut from wire mesh in a tube. In addition to simplicity, these stacks have two significant advantages. First, the wire is relatively impervious to moderately high temperatures and second, the effective thermal conductance of the structure is one to two orders of magnitude lower than a comparable metal "parallel plate" structure. Since no linear theoretical thermoacoustic models exist for these wire mesh stacks, the approach taken was simply to measure the performance of several different mesh stacks. Results gathered from two different prime movers indicate acoustic onset temperatures and amplitude performance comparable to the best data for parallel plate stacks. Moreover, measured efficiencies for mesh stacks appear to be substantially higher than for parallel plates.

TABLE OF CONTENTS

I. INTRODUCTION..1

A. MOTIVATION..1

B. THERMOACOUSTIC ENGINE BASICS..2

1. Some History and a Basic Functional Description..2
2. Penetration Depth (δ_κ)..3
3. Efficiency..4

C. GOALS..6

II. EXPERIMENTAL APPARATUS, INSTRUMENTATION, AND PROCEDURE..7

A. THE OPEN THERMOACOUSTIC PRIME MOVER..7

1. Apparatus..7
   a) Heat Exchangers..8
   b) Thermoacoustic Stack..8
2. Instrumentation..8
3. Procedure..9

B. THE SEALED THERMOACOUSTIC PRIME MOVER..10

1. Apparatus..10
   a) Hot End Tube Assembly..10
   b) Hot Heat Exchanger Assembly..11
   c) Stack Assembly..12
   d) Cold Heat Exchanger Assembly..12
   e) Cold End Tube Assembly..13
2. Instrumentation..13
   a) Thermocouples and Temperature Control..13
   b) Pressure Transducer..14
   c) System Digital Multimeter..14
   d) Personal Computers with GPIB interface..15
3. Procedure..15
   a) Assembly..15
   b) Temperature..16
   c) Measurements..17

III. RESULTS AND DISCUSSION..23

A. THE OPEN THERMOACOUSTIC PRIME MOVER..23

1. Typical Data Run..23
2. Stack Performance Comparison..24
   a) Errors..24
   b) Trends..24

B. THE SEALED THERMOACOUSTIC PRIME MOVER..25

1. Errors..25
2. Data..26
   a) Distortion..27
   b) Amplitude..27
   c) Quasi-Efficiency..27
   d) Frequency..28
   e) Thermoacoustic Heat Input..29

IV. SUMMARY, CONCLUSIONS, AND RECOMMENDATIONS..51

A. SUMMARY..51

B. CONCLUSIONS..52

C. RECOMMENDATIONS..53

LIST OF REFERENCES..55

INITIAL DISTRIBUTION LIST..57

LIST OF SYMBOLS

a	speed of sound
c_p	isobaric specific heat capacity
CHXC	cold heat exchanger center
CHXW	cold heat exchanger wall
$\dot{E}$	resonator dissipation power
Eff_{Quasi}	Quasi-Efficiency
Heater	Electrical power to the heater collar
HHXC	hot heat exchanger center
HHXW	hot heat exchanger wall
HTube	Plunger tube temperature
L	resonator length
Leak	zero acoustic power heat loss
P_m	mean pressure
P_o	dynamic pressure amplitude
Pr	Prandtl number
Q_{Hot}	thermoacoustic heat input
R	resonator radius
Tratio	ratio of averaged absolute hot heat exchanger temperatures to averaged absolute cold heat exchanger temperatures
χ	thermal diffusivity
δ_κ	thermal penetration depth
δ_ν	viscous penetration depth
ε_s	available surface heat capacity
γ	specific heat capacity ratio
η	dynamic viscosity
κ	thermal conductivity
ν	kinematic viscosity

LIST OF SYMBOLS (continued)

ρ	density
ρ_m	mean density
ω	angular frequency

ACKNOWLEDGMENT

This author is forever indebted to a few extremely talented and patient individuals. Specifically I extend my warmest thanks and deepest gratitude to Dr. Tom Hofler, Jay Adeff, Dr. Anthony Atchley, Dr. Robert Keolian, Glenn Harrell, Dr. Dan Holland, and last but foremost my family Karen, Baden, and Luke Reed. Additionally the author would like to acknowledge the financial support of the Office of Naval Research. This work was completed under contract N0001496WR20003.

Dr. Hofler has unquestionably proven, to me personally, his nationally known reputation as a master in the field of thermoacoustics. Your countless hours of patient guidance are deeply appreciated, and it has been one of my highest honors to work under your wing.

If I couldn't make it work or didn't know how to do it, without fail, Jay could and he did. His mechanical and photographic skills seem limitless and always produce to notch quality. Thank you.

When I went prospecting for positive can do guidance for my thesis work, I hit gold in the thermoacoustic group. Dr. Atchley and Dr. Keolian provided hours of fresh, insightful, and unselfish mentoring. This has been greatly appreciated.

Known to all as a machinist extraordinaire, Glenn is a rare gem. If he can help, he will do so in the most polite manor. If he can't do it he will graciously decline, but I have yet to find a job he couldn't handle, and his work is always pristine.

Dr. Holland taught me how to eat, breath, and love physics again. Getting us fleet returnees back in the academic saddle is tiresome and somewhat thankless work, but this Cowboy would like to tip his hat in sincere appreciation.

Without my family, I am just me. With my family we are an unstoppable team. This thesis fruition would be impossible without our team. I extend True Congratulations and Love to my teammates Karen, Baden and Luke.

I. INTRODUCTION

A. MOTIVATION

The Naval Postgraduate School has maintained a nationally known presence on the forefront of a relatively new field of physics, thermoacoustics. The work can be divided into the study of the two classes of thermoacoustic engines. The prime mover uses the thermal heat flow between a heat source and a heat sink to produce high amplitude sound. This acoustic energy is in the form of a standing wave inside a resonator. The heat pump uses the energy of a high amplitude acoustic standing wave to pump heat from a cold heat exchanger to a warmer one. This heat flow is opposite to that expected by normal conduction and is the required process needed for refrigeration. These heat engines each employ a set of hot and cold heat exchangers with material sandwiched between commonly referred to as the "stack." The stack exchanges heat with the cycling gas elements as they flow inside. Notably absent from this description of refrigeration are chlorofluorocarbons (CFC's) and moving parts. Another intriguing idea is the use of waste heat to produce cooling. The US Navy as well as the world will benefit greatly from research and development in this arena.

A near future project of the thermoacoustic group is a thermoacoustically driven thermoacoustic refrigerator having up to one kW of cooling power. It, along with other potential projects, requires improved thermoacoustic engines capable of handling high power densities. This area of thermoacoustics is ripe for discovery with valuable rewards. The high power density prime mover for the heat driven cooler project must operate at high temperatures. Simplicity of fabrication is also a major consideration in this prime mover design. Although the high temperature is not an issue for the refrigeration end, any knowledge gained with prime mover experiments may also apply to the heat pump end.

This thesis is based on the following hunch. Wire mesh screen of stainless steel are used extensively in Stirling engine regenerators. Not only do they work, but they work better than parallel plate geometry, contrary to regenerator theories. Perhaps they

will work as well or better in thermoacoustic stacks as well. The virtues of the wire mesh geometry are ease of fabrication, ability to operate at elevated temperatures, and reduction of the thermal conduction down the stack. The only negative feature is an inability to develop a computational model for this random structure. Intuition superseded the desire for computation and experimentation soon followed.

B. THERMOACOUSTIC ENGINE BASICS

1. Some History and a Basic Functional Description

Thermoacoustic phenomena has been noted and described by several great minds over the last two centuries. Sondhauss, Lord Rayleigh and Kirchhoff just to name a few. Then about 30 years ago Rott [Ref. 1] published the first of a foundational series of papers which lead to a complete theory explaining heat driven oscillations and acoustic heat transport. In the last decade Wheatley, Hofler, Swift, and Migliori greatly expanded the knowledge in this field. Their publications and experiments have put the theory to practice involving thermoacoustic prime movers and heat pumps. Swift [Ref. 2] published a review of these ideas and experiments which has served as reference material for this and many other theses in thermoacoustics.

The thermoacoustic engine is classic in that it is a non-phase-change, reciprocating heat engine. Watt, Stirling, Kelvin, Joule, and Carnot have all extensively studied such engines. The thermoacoustic engine's major ingredients are an acoustic resonator with a standing wave, two heat exchangers, and a stack. It is similar to a Stirling engine in some ways. The first distinguishing component is the resonator, and the second is the stack. The stack is similar to a Stirling regenerator, because fluid flow and fluid pressure oscillate inside. It also serves as a secondary heat storage medium. The stack is unlike a Stirling regenerator for several reasons. In a regenerator the channel size is much less than the thermal penetration depth (δ_κ explained subsequently). Also

the fluid pressure and velocity oscillations are largely in phase. In a thermoacoustic stack the channel size is comparable to δ_κ and the fluid pressure and velocity are roughly 90° out of phase. In parallel plate geometries the optimum channel spacing is usually 3 to 5 times δ_κ.

2. Penetration Depth (δ_κ)

The thermal penetration depth (δ_κ) is the distance heat diffuses through the fluid in one acoustic cycle. Many basic texts like Landau and Lifshitz [Ref. 3] discuss this parameter. It is actually the distance over which temperature oscillations propagating by thermal diffusion fall off by a factor of 1/*e*. It is analogous to the electromagnetic penetration depth commonly called "skin depth." The thermal penetration depth in the acoustic medium is given by

$$\delta_\kappa = \sqrt{\frac{2\chi}{\omega}} = \sqrt{\frac{2\kappa}{\omega\rho\, c_p}}. \qquad (1\text{-}1)$$

In Equation 1-1 χ is thermal diffusivity, ω is angular frequency, κ is thermal conductivity, ρ is density, and c_p is isobaric specific heat capacity.

Similarly there is a viscous penetration depth δ_ν which is the distance the oscillatory shear momentum diffuses through the fluid in one acoustic cycle. More precisely, it is the transverse distance over which velocity falls off by a factor of 1/*e*. Viscous penetration depth is given by

$$\delta_\nu = \sqrt{\frac{2\nu}{\omega}} = \sqrt{\frac{2\eta}{\omega\rho}}. \qquad (1\text{-}2)$$

Here ν is the kinematic viscosity, and η is the dynamic viscosity. The dimensionless ratio of the kinematic to dynamic viscosity defines a fundamental fluid constant known as the Prandtl number Pr.

$$\mathrm{Pr} = \frac{\nu}{\chi}. \qquad (1\text{-}3)$$

The Prandtl number for a single component inert gas is 2/3. By substituting Equation 1-1 & 1-2 into 1-3 the Prandtl number is expressed in terms of the penetration depths.

$$\mathrm{Pr} = \left(\frac{\delta_\nu}{\delta_\kappa} \right)^2 . \tag{1-4}$$

For single component inert gases the ratio of penetration depths is seen to be constant.

$$\frac{\delta_\nu}{\delta_\kappa} = \sqrt{\mathrm{Pr}} = \sqrt{2/3} = 0.83. \tag{1-5}$$

3. Efficiency

In a resonator with a thermoacoustic prime mover but no heat pump, the only acoustic load is caused by friction losses and thermal losses inside the resonator. This cannot be directly measured in our apparatus, so determination of a traditional overall efficiency is not possible. However, we can still attempt a comparison of efficiencies for different stacks. Assume that the stack type is variable, but all other parameters in the resonator are constant. It is reasonable to assume that the resonator will provide a similar loading for each stack. By measuring acoustic pressure amplitudes and thermoacoustic heat input for each stack at the same conditions, an efficiency comparison can be made.

Swift [Ref. 4] derived an equation for the total resonator dissipation power $\dot{E}$ for a plane wave resonator.

$$\dot{E} = \frac{1}{4} \frac{P_o^2}{\rho_m a^2} \omega \pi RL \left[\delta_\kappa \frac{\gamma - 1}{1 + \varepsilon_s} \left(1 + \frac{2R}{L} \right) + \delta_\nu \right]. \tag{1-6}$$

From this, a quasi-efficiency expression can be derived. The above variables apply to the acoustic medium and the inside of the resonator. P_o is the dynamic pressure amplitude, and ρ_m is the mean density. The speed of sound is a, and the angular frequency is ω. The radius and length of the resonator are given by R and L. The thermal and viscous penetration depths, described above, are denoted by δ_κ and δ_ν. The specific heat capacity ratio is γ, and the available surface heat capacity is ε_s.

For this experiment, ε_s for the copper wall is very small compared to 1 and can be ignored. Then by using $\rho_m \; a^2 = \gamma \; P_m$, where P_m is the mean pressure, Equation 1-6 becomes

$$\dot{E} \approx \left(\frac{\pi R}{4\gamma}\right)\left(\frac{P_o}{P_m}\right)^2 P_m \, \omega L \left[\delta_\kappa (\gamma - 1)\left(1 + \frac{2R}{L}\right) + \delta_\nu\right]. \tag{1-7}$$

The geometry of the apparatus is such that the term $2R/L$ is much less than 1 and can be ignored. From Equation 1-5, $\delta_\kappa = \delta_\nu / \sqrt{\Pr}$. Therefore

$$\dot{E} \approx \left(\frac{\pi R}{4\gamma}\right)\left(\frac{P_o}{P_m}\right)^2 P_m \omega L \delta_\nu \left[\left(\frac{\gamma - 1}{\sqrt{\Pr}}\right) + 1\right]. \tag{1-8}$$

Eliminating all the constants Equation 1-8 can be written as a proportionality.

$$\dot{E} \propto \left(\frac{P_o}{P_m}\right)^2 P_m \omega L \delta_\nu . \tag{1-9}$$

From Equation 1-2, viscous penetration depth $\delta_\nu = (2\eta/\omega\rho)^{1/2}$. Since the dynamic viscosity η is nearly independent of the pressure then $\delta_\nu \propto (\omega \; \rho_m)^{-1/2}$ or $\delta_\nu \propto (\omega \; P_m)^{-1/2}$. Proportionality 1-9 then becomes

$$\dot{E} \propto \left(\frac{P_o}{P_m}\right)^2 L (\omega \; P_m)(\omega \; P_m)^{-1/2} = \left(\frac{P_o}{P_m}\right)^2 L \sqrt{\omega \; P_m} . \tag{1-10}$$

Note that the L dependence is for a constant diameter resonator at uniform temperature. In this case $\omega \propto 1/L$, so then

$$\dot{E} \propto \left(\frac{P_o}{P_m}\right)^2 \frac{1}{\omega} \sqrt{\omega \; P_m} = \left(\frac{P_o}{P_m}\right)^2 \sqrt{\frac{P_m}{\omega}} . \tag{1-11}$$

Finally a quasi-efficiency term is reached by the ratio of resonator dissipation power to the thermoacoustic heat input.

$$Eff_{Quasi} = \frac{\dot{E}}{Q_{Hot}} \propto \frac{\left(\frac{P_o}{P_m}\right)^2 \sqrt{\frac{P_m}{\omega}}}{\mathrm{Q}_{\mathrm{Hot}}} . \tag{1-12}$$

C. GOALS

The first goal of this thesis was to produce sound in a thermoacoustic prime mover which employed wire mesh screens as stack material.

Second was to accurately measure the parameters of the acoustic wave produced. It was decided that the performance of the wire mesh stack should be compared to a reference stack. The reference stack chosen was a typical polyester spiral roll stack described in Chapter II. Measurements of acoustic amplitude, amplitude ratio to mean pressure, and heat load were needed. An efficiency comparison, discussed above, could be derived from the measured variables.

The final goal was determination of the optimum mesh sizing relative to δ_κ.

II. EXPERIMENTAL APPARATUS, INSTRUMENTATION, AND PROCEDURE

Two series of experiments were conducted. The first series made use of an open quarter wavelength prime mover. This simple apparatus allowed quick testing of many different stacks. The second more detailed set of measurements were conducted in a sealed half wavelength prime mover. This series involved more precisely controlled testing yielding better data for more reliable comparison. Also, new information in the form of heat power measurements was collected in the sealed half wavelength prime mover.

A. THE OPEN THERMOACOUSTIC PRIME MOVER

1. Apparatus

Figure 2.1 shows the Hofler tube [Ref. 5] used in the preliminary experiments. It is a quarter wavelength resonator tube open to the atmosphere on the cold end. This prime mover was chosen for the initial series of experiments because of its simplicity. It has very few parts, is extremely portable, and requires only minutes to change stack material.

Unlike the sealed prime mover, described later, the open prime mover uses air as the acoustic medium. Thus it requires no hermetic gas seals, no gas purging and no leak detecting during assembly. The few parts bolt together with greased flat face seals on the flange faces providing the acoustic seal. Although simple, this seal must be made carefully as particulates or inadequate grease can lead to a flange leak and reduced acoustic amplitude at the open end.

Additional simplicity comes from the use of external thermocouples only. Internal thermocouples would provide more accurate measurements but add complexity, which is not desired in this apparatus.

a) Heat Exchangers

The two heat exchanger units are integral parts of the hot and cold sections of the resonator. They [Ref. 6] consist of a circular finned element soldered into the hot and cold section tube flanges. The finned element consists of parallel copper fins bonded at their ends to a thin circular ring of electroplated copper.

b) Thermoacoustic Stack

During this series of experiments, one polyester and many wire mesh stacks were tested. A typical polyester stack was used as the reference stack. It [Ref. 7] consists of a long strip of polyester film with fishing line spacers glued to the surface. The strip is then wound in a spiral roll. The wire mesh screens were fabricated from double crimp weave stainless steel wire screen. Mesh sizes (number of wires or openings per lineal inch) ranged from 10 to 28. Wire diameters ranged from 7.5 to 23 mil. The standard market grade mesh is referred to as the standard mesh. A fine wire grade mesh which has smaller diameter wires than standard wire cloth is referred to as bolting cloth. Standard cloth having 18 wires per inch is denoted as "Std 18," while bolting cloth with 10 wires per inch is referred to as "Bolt 10". The wire mesh stacks were made by stacking circular cut mesh screens until the stack holder tube was filled. The disk shaped screens are generally not perfectly flat, and the stack holder tube must be packed with screens under modest force to ensure a dense packing. The screen orientation is random. Some experimentation was conducted using wire spacers placed between bolting 18 mesh screens. Figure 2.2 shows examples of polyester and wire mesh stack.

2. Instrumentation

Thermocouples were attached on the outside of the resonator tube near each heat exchanger providing a rough measurement of their temperatures. A condenser microphone [Ref. 8] was used to record the sound amplitude external to the tube. A digital oscilloscope [Ref. 9] was used to capture the waveform and measure its

characteristics; most importantly the frequency, Root Mean Squared (RMS) amplitude voltage, and the Fast Fourier Transform (FFT). A portable computer stored this waveform and scope measurement information which it gathered via the General Purpose Interface Bus (GPIB). A digital multimeter (DMM) [Ref. 10] was used as a backup to verify proper RMS amplitude voltage.

3. Procedure

Measurements were conducted in an anechoic chamber designed to absorb at least 99% of all reflected sound above 100 Hz. The microphone was positioned on the tube axis and one half meter from the open end of the tube. It was checked-out and calibrated with a pistonphone [Ref. 11] daily. The open end of the resonator tube was submersed in liquid nitrogen until its temperature equalized with the bath. It then was removed, and a piece of cloth was inserted in the open cold end of the tube. The cloth provided sufficient acoustic damping to prevent the onset of sound oscillations. With the hot end at 10° C and the cold end at −170° C, the damping cloth was removed from the open tube end. Thermoacoustic sound generation commenced (referred to as onset) and was measured.

The oscilloscope was preset to trigger at the start of the sound. The first half second of sound was recorded and analyzed. The growth part of the waveform was ignored and approximately 50 cycles were used for the measurements. At about one half second the prime mover "wind" hit the microphone and caused low frequency noise.

Additionally the thermocouple readings were recorded when the sound stopped (referred to as shutoff). Sound shutoff is the point at which the sound amplitude drops effectively to zero and occurs when the temperature difference across the stack decreases to a point where the sound generating power of the stack is less than that required to overcome the acoustic losses of the rest of the system.

Twenty-six data runs with eighteen different stacks were conducted. These results were analyzed for best performance. The highest amplitude stacks were selected for more detailed measurements in the closed prime mover.

B. THE SEALED THERMOACOUSTIC PRIME MOVER

Figure 2.3 and 2.4 show the assembly of the sealed prime mover. It is a half wavelength sealed resonator that is designed to use low variable pressure neon gas. This allows relatively low input heater power with high acoustic amplitudes. The adjustable pressure permits adjustable penetration depth. This sealed system required many assembly hours ensuring proper hermetic gas seals, performing gas purges, and conducting leak detection checks.

Unlike the open prime mover experiments, precise measurements were desired requiring more complicated instrumentation. An internal pressure transducer at the hot end was used for measuring both the internal mean pressure and the dynamic acoustic amplitude. Thermocouples were used internally and externally. Their locations are described below under instrumentation.

A summarized top to bottom description follows. This apparatus was largely the same as that used in Castro's thesis [Ref. 12].

1. Apparatus

a) Hot End Tube Assembly

Figure 2.3.a shows the movable plunger assembly. A sliding piston with O-ring groove is fixed to the end of a threaded rod. The piston has penetrations for a transducer and gas line. A pressure transducer with an O-ring seal is threaded into the piston allowing internal pressure measurements.

The pressure transducer [Ref. 13] is a silicon piezoresistive type, with an integral evacuated reference volume. The transducer measures both the absolute static pressure inside the apparatus as well as the dynamic acoustic pressure. The dynamic response of the transducer is flat for frequencies below 1 kHz.

The gas line is soldered in place and has a capillary insert. This allows internal pressure control yet provides an extremely high acoustic impedance coupling,

which ensures good acoustic isolation from the gas line. The threaded rod and gas line are attached to a support bracket. The gas line is fitted with an isolation valve. The end cap rests on the upper end of the plunger tube. Two nuts on the threaded rod above the end cap are used for plunger positioning. The sealed resonator operates below atmospheric pressure drawing the plunger down. The nuts contact the end cap and fix the plunger position. A retaining ring is clipped onto the threaded rod below the end cap. This is attached just above the transducer to prevent transducer damage if the tube internal pressure rises above atmospheric and the plunger is pushed out. The end cap is fastened to the plunger tube via the upper end-cap clamp as shown in Figure 2.4. This movable plunger assembly is inserted into the upper tube.

Figure 2.3.b shows the upper tube assembly. The movable plunger has free travel down most of the length. Near the bottom are the thermocouple penetrations. These are made through the upper tube flange. This flange is soldered to the upper tube and is fitted with an O-ring grove on the lower face. There are five radial thermocouple penetrations fitted with feed-through inserts which are soldered to the flange. Pressure tight seals are made by epoxy and wax between the bare thermocouple wires and the inserts. Inside the tube are connection panels which allow easy solder connection of thermocouple wire leads with feed-through wire leads. A bolt circle consisting of eight clearance holes in the tube flange provide mounting to the hot heat exchanger.

b) Hot Heat Exchanger Assembly

Figure 2.3.c shows the hot heat exchanger. It provides heat to the stack from a clamp-on heater collar as shown in Figure 2.4. The heat exchanger unit is similar to that of the open prime mover and consists of a circular finned element soldered into a mounting flange. The finned element consists of parallel copper fins bonded at their ends to a thin circular ring of electroplated copper. This flange is flat on the top since it seals with the O-ring from the lower face of the plunger tube flange. The bottom face of the hot heat exchanger flange has an O-ring grove for sealing with the upper flange of the stack holder.

c) *Stack Assembly*

Figure 2.3.d shows the stack holder. It holds the stack material which is in contact with the hot and cold heat exchangers on opposite ends. The stack holder tube is a short piece of thin-wall stainless steel tubing. This minimizes thermal conduction down the wall. Flanges on top and bottom are tapped with eight machine screw holes for mounting.

During this series of experiments, three different stacks were tested. The polyester stack used in Castro's thesis was used as the reference stack. The polyester stack consists of a long strip of polyester film with fishing line spacers glued to the surface. The strip is wound in a spiral roll. Construction of this stack is similar to the polyester stack used in the open prime mover. This stack is referred to as the "Poly" stack throughout this thesis. The performance of the Poly stack and two wire mesh stacks were measured. These two mesh stacks were the ones that performed the best in the open prime mover experiments. One was fabricated from bolting cloth having 16 wires per inch, which we will refer to as "Bolt 16," and the other stack used bolting cloth with 10 wires per inch, referred to as "Bolt 10." Fabrication of these stacks was similar to that described for the open prime mover.

d) *Cold Heat Exchanger Assembly*

Figure 2.3.e shows the cold heat exchanger. It removes heat from the stack as it is exposed to liquid nitrogen temperatures. This heat exchanger is very similar to the hot heat exchanger except it has no O-ring groves. O-ring seals are unreliable at liquid nitrogen temperatures. As seen in Figure 2.3.d a Teflon™ gasket provides a simple and effective, but low thermal conduction seal between the heat exchanger flange and the stack holder. Figure 2.3.e shows the lead wire seal which provides a high thermal conduction seal between the cold heat exchanger and the cold collar of the resonator. Figure 2.3.f shows the assembly of the aforementioned components into the cold end of the resonator.

e) Cold End Tube Assembly

Figure 2.3.g shows the cold end of the resonator. It is the heat sink for the cold heat exchanger and is largely responsible for the frequency characteristics of the internal standing wave. It was designed by Castro and is shaped to shift the frequencies of the second and third modes relative to the fundamental, so that these modes are not harmonics of the fundamental. This prevents the severe shock wave formation measured by Castro and promotes a sinusoidal waveform. The cold collar and fingers improve the heat transfer from the cold heat exchanger to the liquid nitrogen. The cold end assembly is submersed in liquid nitrogen. The dewar level is maintained near the top of the cold collar. Figure 2.3.h shows the total sealed prime mover.

2. Instrumentation

Figure 2.5 shows the instrumentation used for the sealed thermoacoustic prime mover experiment.

a) Thermocouples and Temperature Control

Type E thermocouples were used both internally and externally. The internal thermocouples were attached to the hot and cold heat exchangers. Two thermocouples were soldered to each heat exchanger. The contact points were at the center and the internal wall as shown in Figure 2.5. The average of these two readings was used as the overall heat exchanger temperature. At high heater power levels a temperature difference between the wall and the center develops due to the thermal characteristics of the heat exchanger.

Other thermocouples are attached externally as shown in Figure 2.5. Their positions are at the wall of the hot plunger tube, the heater collar attachment screw, and the cold collar finger attachment screw. A thermocouple scanner [Ref. 14] was used to sample these thermocouples.

An additional thermocouple was fitted into a machined slot in the heater collar. This was used as feedback for the temperature controller. A temperature controller [Ref 15] was used to control the power to the heater collar. Power to the heater collar was supplied by a DC power amplifier [Ref. 16].

Thermocouple wire diameter varied. Internal wires were 3 mil providing minimal disturbance of flow. All feed-throughs and most external wires were 5 mil providing improved strength and lower resistance. The exceptions were the heater collar thermocouples which used 35 mil wire.

b) Pressure Transducer

A piezoresistive type pressure transducer [Ref. 13] penetrated the hot end plunger piston as shown in Figure 2.5. Its output was filtered through a precision bridge conditioner box which was custom made. Both the AC and DC responses were measured, and the ratio of the dynamic to mean pressure was computed as a primary data output. This amplitude ratio provides an accurate value independent of transducer sensitivity. Also of note was that the AC response was flat beyond 1kHz.

The manufacturer's DC response calibration values were verified with agreement to within 0.2%. Using a mechanical pump, the transducer was subjected to a vacuum of less than 15 Pa, and the "zero" response was measured. Then it was exposed to the local atmospheric pressure, and a full scale response was measured. A barometer [Ref. 17] was used to correct the atmospheric value, and a full scale sensitivity was determined. Linear response was assumed.

c) System Digital Multimeter

A digital multimeter [Ref. 18] was used to measure pressure, frequency, and heater power parameters. The AC and DC voltages from the pressure transducer preamplifier provided the AC and DC pressure signals. Frequency was measured from the AC pressure signal. Heater DC voltage and current was measured as shown in Figure 2.5. The current resistor was a precision 0.2 ohm resistor.

d) Personal Computers with GPIB interface

A personal computer with Microsoft Windows NT™ operating system was used for data gathering. A program written in the C language was used to gather all data via GPIB interface from the temperature scanner and the digital multimeter. The program sent data real-time to the screen and storage disk in the form of a scrolling log. Each data line contained the time, all thermocouple readings, mean pressure, dynamic to mean pressure ratio, frequency, and computed heater power. A digital oscilloscope [Ref. 9] was used to capture the waveform and verify the digital multimeter frequency value. A portable computer stored this waveform and scope measurement information.

3. Procedure

a) Assembly

Assembly, leak checks, and gas purges of the sealed prime mover took six to ten hours. This was longer than the time required for measurements.

The components of Figure 2.3 were assembled, as shown in Figure 2.4, from the bottom up. The cold heat exchanger flange was sealed on the bottom side with a lead wire seal and on the top by a Teflon™ gasket. This ensured good thermal contact between the cold collar and the cold heat exchanger flange. The Teflon™ seal is simpler to use and is relatively free of voids or gaps that may cause acoustic dissipation. Stack material was then inserted into the holder, and the thermocouples leads were inserted up through the hot heat exchanger. The hot heat exchanger has o-ring seals on both flange faces. These provide simple and reliable seals at room temperatures while ensuring good thermal contact.

Leak checks were performed three times during assembly using a helium leak detector [Ref. 19]. The resonator, cold heat exchanger, and stack holder were assembled and checked. Eight screws attached these components and provided the force to crush the lead wire seal. This required a torque pattern which was repeated numerous

times. The plunger tube with its thermocouple feed-throughs were leaked checked. These proved to be the most time consuming seals to make. The feed-through wires were then soldered to the hot and cold heat exchanger thermocouple leads. The plunger tube, hot heat exchanger, and stack holder were attached by another eight screws, and the assembled unit was again leak checked. Finally the plunger assembly was inserted into the plunger tube. The gas line of flexible tubing and the microphone wires were connected.

The entire sealed prime mover was purged using a vacuum pump, neon gas and a custom built pressure control panel. The prime mover was alternately evacuated to 7 kPa and filled to 160 kPa of neon. This cycle was repeated five times and was finished with the prime mover mostly evacuated. This low pressure state was desirable because acoustic onset is impossible at any of the accessible cold temperatures.

Insulation was then added externally. The stack holder and hot end were wrapped with insulating material. Cork and insulation collars were placed at the top of the dewar and the prime mover was inserted. The dewar was supported at its opening by a padded clamping ring. The prime mover rested on this ring with the cork and insulation collar sandwiched between the two. This insulation scheme was used to minimize heat losses to the environment and redirect the cold liquid nitrogen vapor from convectively cooling the hot end. All hot end components were designed to minimize thermal mass. In addition to increasing heat loss this excess mass causes slow temperature response and poor controller stabilization.

b) Temperature

A large temperature span is used for this sealed prime mover in order to achieve very high relative acoustic amplitudes. While extremely large amplitudes were more important for the Castro heat exchanger measurements than for these stack measurements, these amplitudes are relevant and not unwelcome. A controlled variable temperature span apparatus would have been preferable, but time was not available to add the necessary complexity.

The temperature span is established and maintained as constant as possible. Liquid nitrogen is added to the dewar, and cold end equilibrium is reached at approximately –194° C. This temperature was maintained during the experiment by a trickle flow of liquid nitrogen to keep the dewar full. This flow required slight adjustments as acoustic power was generated and heater power varied. The warm end was maintained just above room temperature (approximately 35° C) by adjusting the heater controller parameters. Establishing stable parameters required significant experimentation. Once acoustic generation commenced, heat flow increased, and some temperatures did vary (see Chapter III). Prior to the commencement of acoustic sound generation (onset), heater power was measured to establish the heat loss value at zero sound level.

c) Measurements

Data was gathered over several days with disassembly and assembly required when the stack material was changed. Three different stacks were tested, with approximately the same conditions, allowing direct comparison of the results. Pressure and piston position parameters were varied and data was gathered automatically as described in the instrumentation section. First mean pressure was varied in steps from onset to just below atmospheric pressure. This was done at three different piston positions. Then at a fixed pressure of 50 kPa the piston position was varied over its full range of about 15 cm. This had the effect of changing the position of the stack and heat exchangers relative to the hot end pressure antinode. At all data points heater power and other parameters were allowed to equilibrate. Results are contained in the Results and Discussion Chapter III.

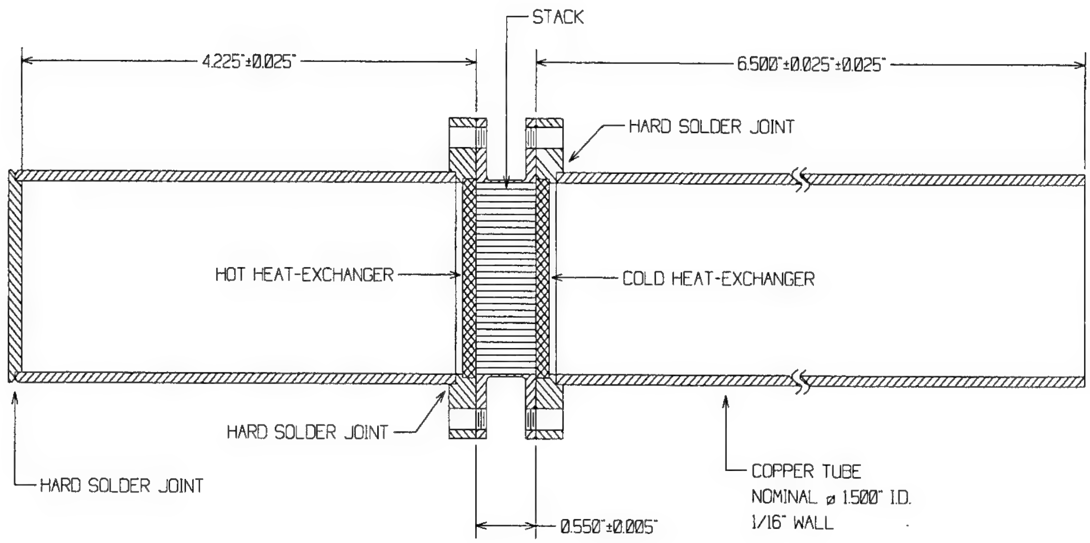

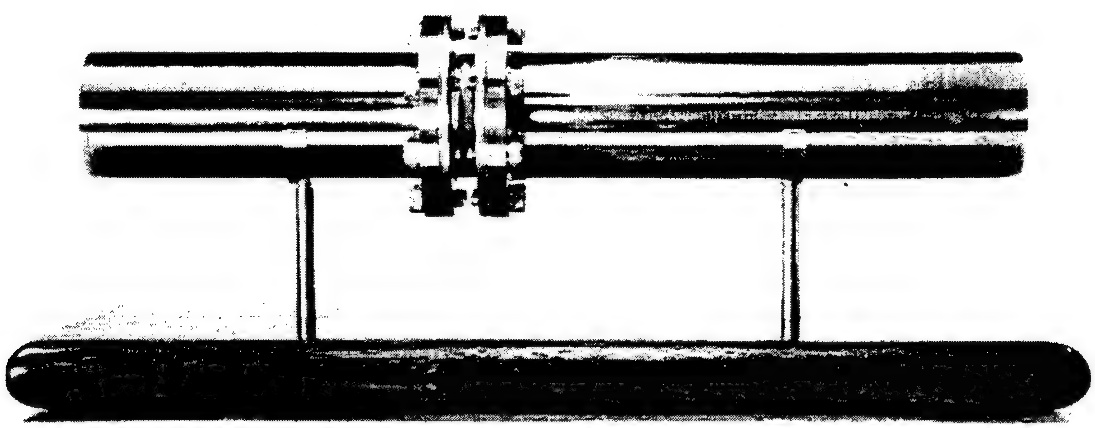

Figure 2.1 Open Thermoacoustic Prime Mover (Hofler Tube)

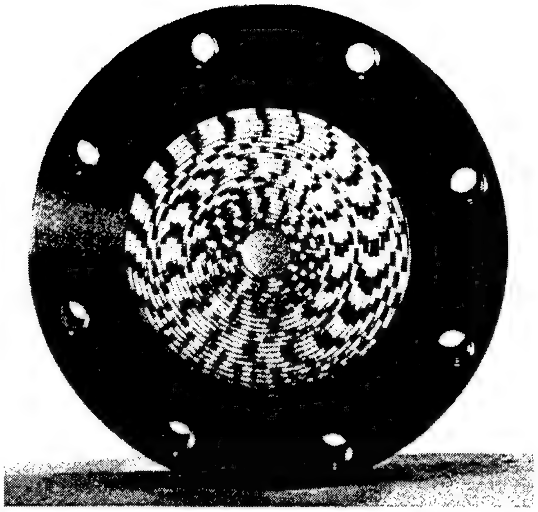

a) Polyester spiral stack

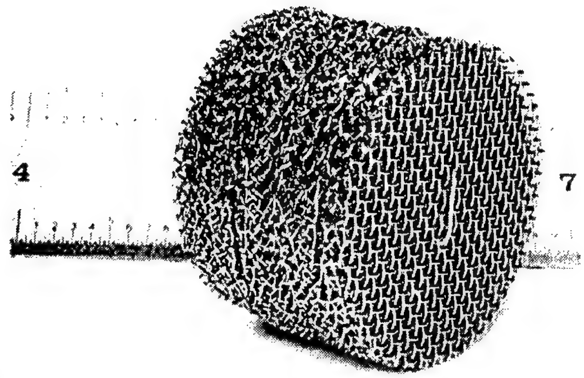

b) Wire mesh stack

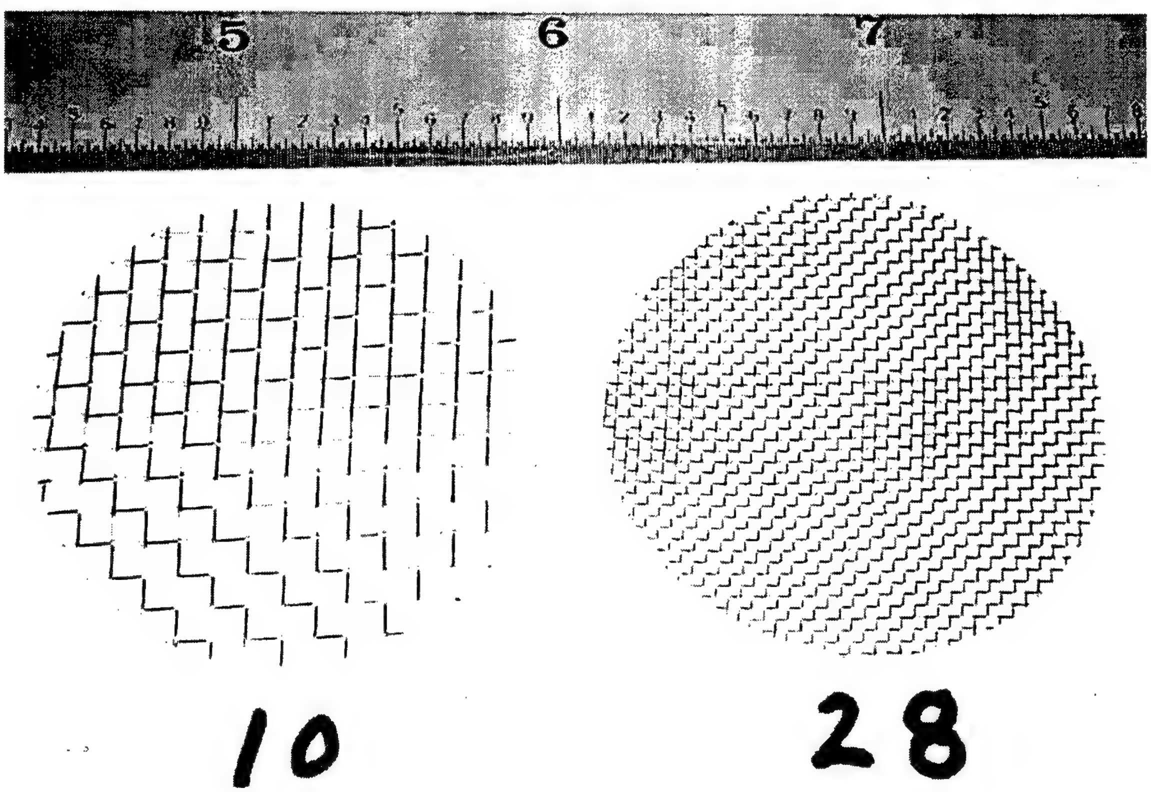

c) Range of meshes tested

Figure 2.2 Thermoacoustic Prime Mover Stack Material

a) Plunger Assembly

b) Upper Tube Assembly

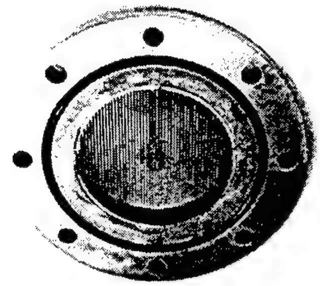

c) Hot Heat Exchanger

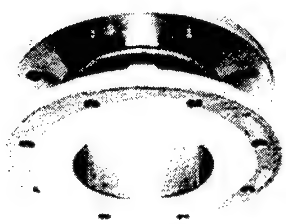

d) Stack Holder

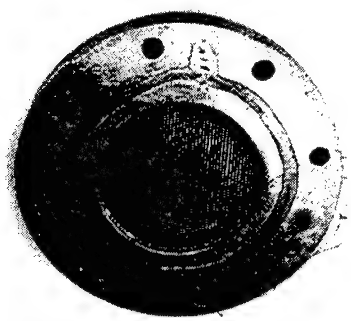

e) Cold Heat Exchanger

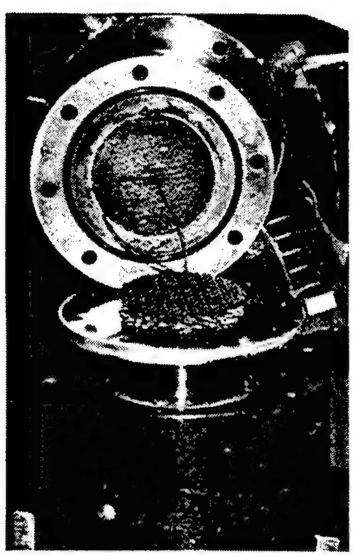

f) Stack & Heat Exchanger Assembly

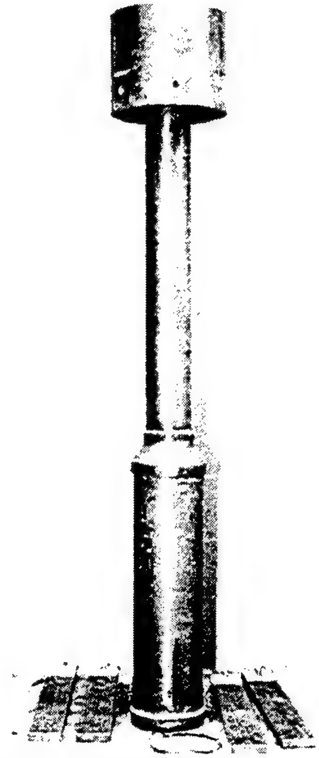

g) Cold End Resonator

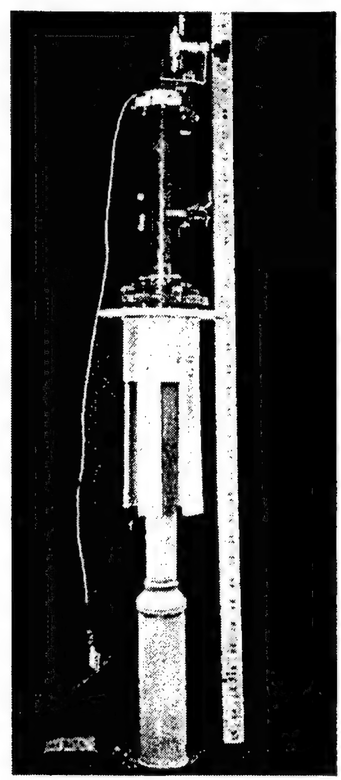

h) Sealed Prime Mover

Figure 2.3 Sealed Thermoacoustic Prime Mover Assembly

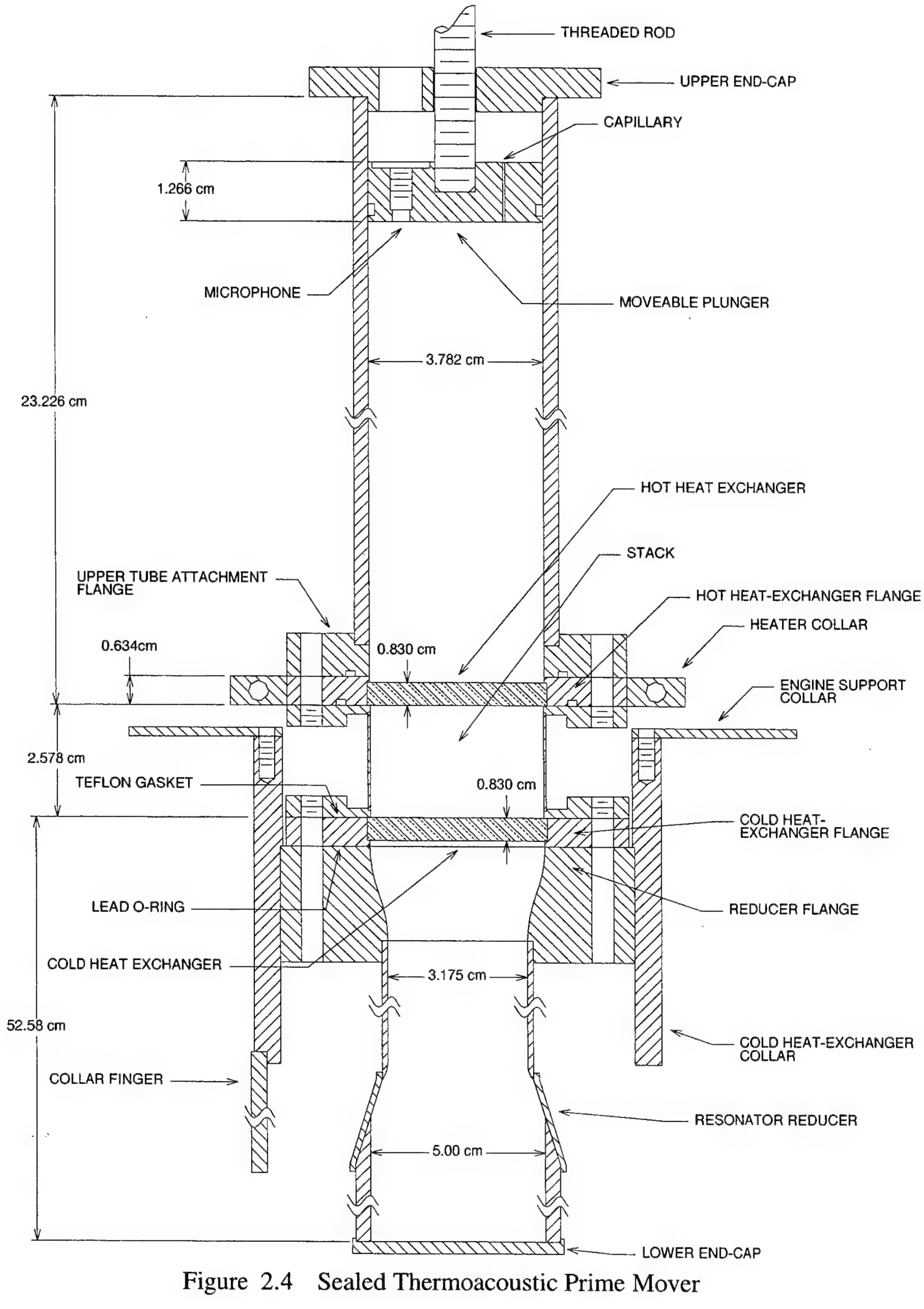

Figure 2.4 Sealed Thermoacoustic Prime Mover

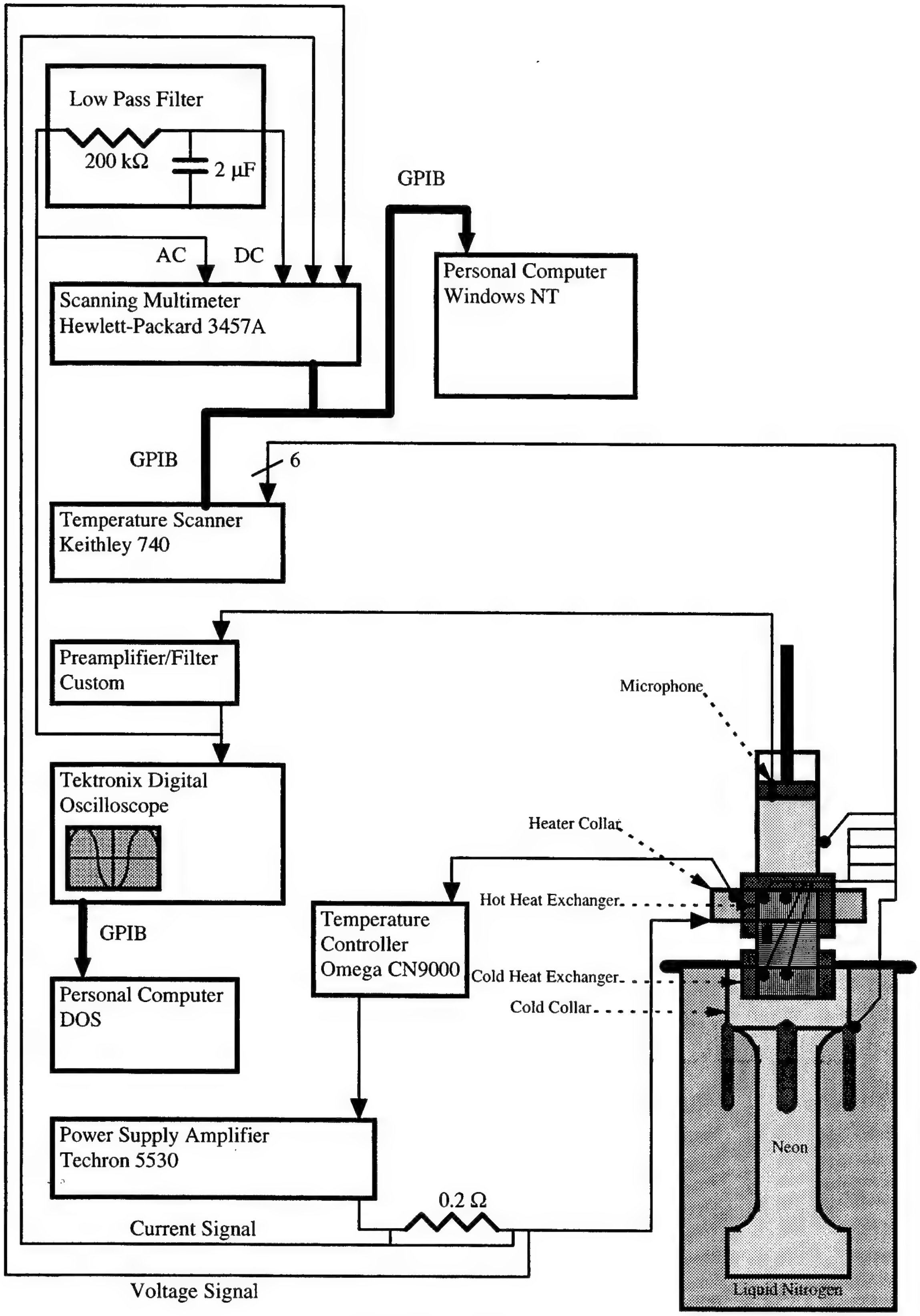

Figure 2.5 Sealed Prime Mover Instrumentation

III. RESULTS AND DISCUSSION

This Chapter discusses the results of the two series of experiments. First are those from the open quarter wavelength prime mover, and second are those from the sealed half wavelength prime mover. Theory, apparatus and procedural details previously discussed are not repeated.

A. THE OPEN THERMOACOUSTIC PRIME MOVER

The first trial of a wire mesh stack delivered a quick start to this thesis work, as high amplitude sound emitted from the open thermoacoustic prime mover. The sound produced was compared to that of the typical polyester roll stack. With the wire mesh stack installed, two additional sound characteristics were noted. The first was a "buzzing" sound and proved to be related to insufficient packing density of the screens. The second is best described as a "hollow and somewhat irritating" sound. It was suspected that this quality could be readily measured as harmonic distortion of the sound pressure waveform. The waveform data gathering described in Chapter II was required in order to prove this suspicion.

1. Typical Data Run

Figure 3.1 is representative of the data gathered for each of the 26 runs. Standard 20 wire mesh was the stack material used to produce the sound data of Figure 3.1. These are direct images of the digital oscilloscope [Ref. 9] screen. The first one shows initial sound generation as the damping rag is removed. The second one displays the possible oscilloscope measurements available using its "Snapshot" function. Thirdly is an FFT of the waveform. The Snapshot and FFT are of a selected portion of the waveform. This portion is selected by using the oscilloscope's "Gating" function. Finally is an image of the expanded waveform. This is representative of the distorted

square waveforms produced by the mesh screens having relatively more wires per lineal inch (18 to 28 mesh). Figure 3.2 is presented for comparison showing the near sinusoidal waveforms of the polyester stack and the most open mesh stack tested, bolting 10. Since the distortion in the waveforms for different mesh stacks was varied, amplitude measured in terms of RMS voltage (V_{RMS}) was chosen as the best measure of stack performance.

2. Stack Performance Comparison

Twenty six stacks were assembled and tested. Table 3.1 contains the details of each stack and its measurements. Figure 3.3 is a plot of amplitude versus porosity. Amplitude was measured in mV_{RMS}. The highest measured amplitudes were about 40 mV which corresponds to 106 dB SPL at the microphone. The porosity is the ratio of gas volume to total volume of each stack. Many variables affect stack performance, but the trends of Figure 3.3 indicate that the dependence on porosity is significant.

a) Errors

These measurements were taken sporadically over a period of two months. After initial measurements showed an improved performance with more open mesh, a second wire mesh purchase was necessary. Also during this time period the apparatus was loaned to another research lab. Upon return and re-assembly some results were irreproducible. The results were not grossly different, but the best performing meshes were re-measured to ensure adequate comparative choices could be made. These variations and the uncontrollable acoustic medium, air at atmospheric pressure and local humidity, cause some fluctuations in the results.

b) Trends

Both the standard and bolting cloth meshes indicate a trend leading to the conclusion that fewer wires per inch is better. The bolting cloth out performs the standard mesh indicating that less metal and more open area is best. Some bolting 18

mesh stacks employed spacers. Some spacers had the approximate thickness of a single mesh screen while others had the thickness of two mesh screens. The stack denoted Bolt 18.f was assembled with a pattern of two screens to one spacer. Stacks Bolt 18.e and Bolt 18.g were constructed by alternating screens and spacers, one to one. Spacers provided a small yet discernible amplitude increase but had a higher shutoff ΔT.

After reviewing these results bolting 10 and 16 were chosen for more detailed measurements in the sealed thermoacoustic prime mover.

B. THE SEALED THERMOACOUSTIC PRIME MOVER

This series of experiments was performed to gather detailed measurements on bolting 10 and bolting 16 wire mesh stacks. They were compared to the reference polyester stack of Castro's thesis. The experiments were conducted over a two week period. The majority of that time was spent in assembling the apparatus. The data collection required approximately 30 hours and produced some 6000 lines of data. The transient measurements were removed, and the steady state data was averaged, and then reduced to that presented in Table 3.2.

1. Errors

All data was very accurate with the exception of some heater powers. Temperature, pressure voltages, and frequency values were accurate to less than one tenth of a percent. The zero sound heater power was slightly variable. The temperature controller stability was usually good but occasionally erratic. Near steady state, heater powers varied by as much as 10 to 20 watts, yet sometimes the variation was less than 1 watt. After averaging many lines of data at each data point, heater power errors were estimated at 1%.

During the experiments and data reduction several values were checked to ensure good steady state values were obtained. Frequency was checked before, during and after

the data runs to ensure the pure neon acoustic medium was not contaminated. The pressure and plunger position were varied frequently, and an air leak past one of the seals would ruin the data. Valid steady state values were obtained by first verifying the cold collar temperature and heater power readings were steady. The hot and cold heat exchanger temperatures were then checked, to ensure the thermoacoustic heat input was steady.

When the mean pressure was decreased to below sound shutoff, the heater power did not go to zero. This was due to heat leakage down through the stack and to the environment. This heat leak varied from 14 to 17.5 watts. The "thermoacoustic heat input" was determined by subtracting this heat leak from the heater power values at each data point. This thermoacoustic heat input is abbreviated as Q_{Hot} throughout this thesis.

While the value of the heat leak could be stated as being 16.0 ± 1.0 watts, the leak value was measured frequently, usually after a small number of data points were taken, and thus the estimated heat leak uncertainty for each data point is closer to ± 0.5 watt. Since the Q_{Hot} value is obtained by differencing two values, both having significant errors, the resultant errors for Q_{Hot} vary substantially. The error in Q_{Hot} is estimated to be less than 2% for values above 40 watts, although increasing to 10% for $Q_{Hot} = 5$ watts, and increasing rapidly for values below 5 watts. A few data points above 130 watts may have errors in the range of 4% because of temperature controller stability problems. The percentage error in the quasi-efficiency values discussed below is identical to the percentage error in Q_{Hot}.

2. Data

The data obtained was reduced and is presented in Table 3.2. The significant variables were the stacks, the mean pressure, and the plunger to stack distance. The three stacks are denoted as Poly, Bolt10, and Bolt16. Variable mean pressure data was taken at three different fixed plunger positions. Variable plunger position data was taken at a fixed pressure of 50 kPa.

a) Distortion

Heater powers of about two hundred watts produced acoustic pressure amplitudes which were nearly 30% of the mean gas pressure. These levels were easily audible external to the sealed prime mover. At these high acoustic amplitudes distortion was apparent in many cases. Waveforms for the Poly and Bolt10 stacks are shown in Figure 3.4. The waveforms were most distorted at the shortest plunger distances. The acoustic power in this measured distortion is less than 1.5%. These waveform distortions are similar to those seen in a Stirling engine regenerator [Ref. 20]. At longer plunger distances the bolting 16 stack exhibited significantly more distortion than the Poly stack, as shown in Figure 3.5. Note the relatively low distortion for the Poly stack. This was typical for the Poly stack except at the shortest piston distances. This can be seen by comparing Figures 3.4 and 3.5.

b) Amplitude

Figures 3.6 and 3.7 are amplitude plots expressed using the dimensionless percentage ratio of dynamic to mean pressure. The RMS pressure amplitude is used instead of the more typical peak value. Because of the varied amount of distortion in the waveforms, this was considered a better value for comparison. Figure 3.6 shows a strong positive dependence on mean pressure at low pressures and asymptotic approaches to different plateaus at higher pressures. Both Figures 3.6 and 3.7 show a strong negative dependence on plunger to stack distance. All amplitudes are very high with the Poly stack having the highest.

c) Quasi-Efficiency

Just as interesting but more unexpected was the efficiency data. The quasi-efficiency Equation 1-12, derived in Chapter I, was used.

$$Eff_{Quasi} = \left(\frac{P_o}{P_m}\right)^2 \sqrt{\frac{P_m}{\omega}} \Big/ Q_{Hot} \, .$$

It assumes a linear system where expressions related to power exhibit a quadratic amplitude dependence. It also accounts for pressure and frequency variations. Since the only acoustic load is that associated with losses inside the resonator, which could not be measured, no attempt was made to determine a more traditional overall efficiency in terms of purely measured values. Instead the ratio used assumes like loading for each of the different stacks and is intended to be used for comparison purposes only. All values computed were scaled by a factor of 10^4 before plotting.

Figures 3.8 and 3.9 show the wire mesh stacks are markedly more efficient than the Poly stack. All stacks show significant improvement in efficiency as the plunger to stack distance is minimized. This may be due to the positioning of the stack and heat exchangers closer to the velocity node. This results in less viscous losses and thus higher efficiency. Also the wire mesh's margin of superior performance increases as plunger to stack distance decreases. There is also an improvement in quasi-efficiency for all stacks as pressure is decreased. This trend is apparent from the amplitude plot, Figure 3.6, which shows rapidly increasing amplitudes at the lower mean pressures. The lowest mean pressure data points for quasi-efficiency, Figures 3.7 and 3.9, become erratic as the pressure amplitude ratio and the thermoacoustic heat input value both approach zero. These affect the numerator and denominator of the quasi-efficiency Equation 1-12.

d) Frequency

As expected, Figure 3.10 shows that the frequency inside the resonator has a major dependence on plunger position. A secondary dependence is also expected but less definable. This is the frequency relation to the temperature of the acoustic medium. The hot end gas temperature was estimated by the average of the center and wall hot heat exchanger thermocouples. Figure 3.11 shows the relatively small frequency shift due to gas temperature variations.

e) Thermoacoustic Heat Input

Figures 3.12 and 3.13 show the dependence of the thermoacoustic heat input Q_{Hot} to variations in pressure and plunger to stack distance. The relations are not linear but still of interest. The denominator of the quasi-efficiency Equation 1-12 is Q_{Hot}. As the pressure or plunger to stack distance increases, Q_{Hot} increases causing quasi-efficiency to decrease. Note also that the Poly stack requires substantially more heat input for a modest pressure amplitude advantage. Figure 3.14 shows there are constant thermal resistances in the heat exchangers between the external measurement thermocouples and the internal thermocouples on the fins. The external temperatures are held constant. For all stacks at various positions, as the heat load increases, the thermal resistances cause the hot and cold internal temperatures to converge more or less linearly.

Standard 20 wire mesh stack (16 mil wire, 21 screens), starting ΔT 181 °C, atmospheric pressure

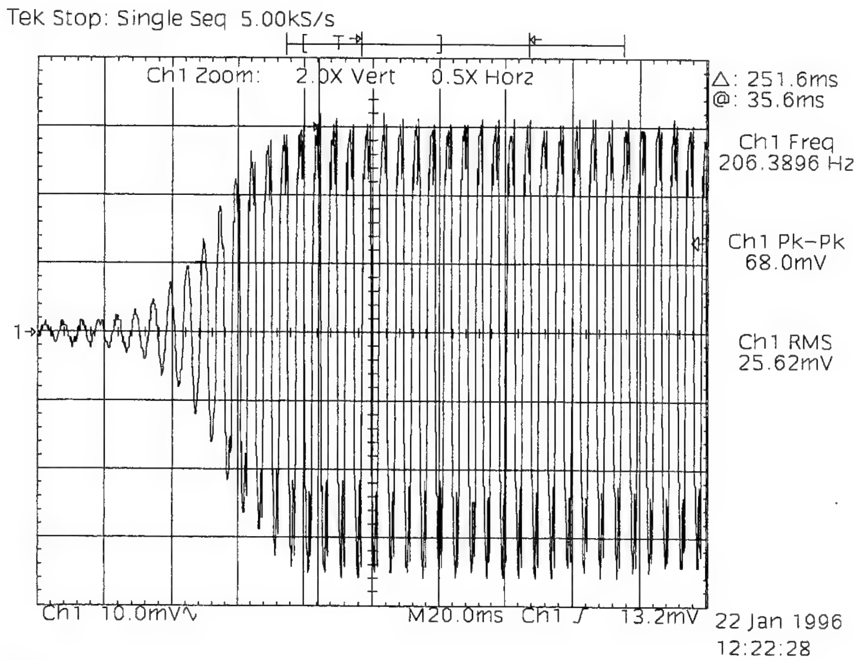

a) Sound initiation

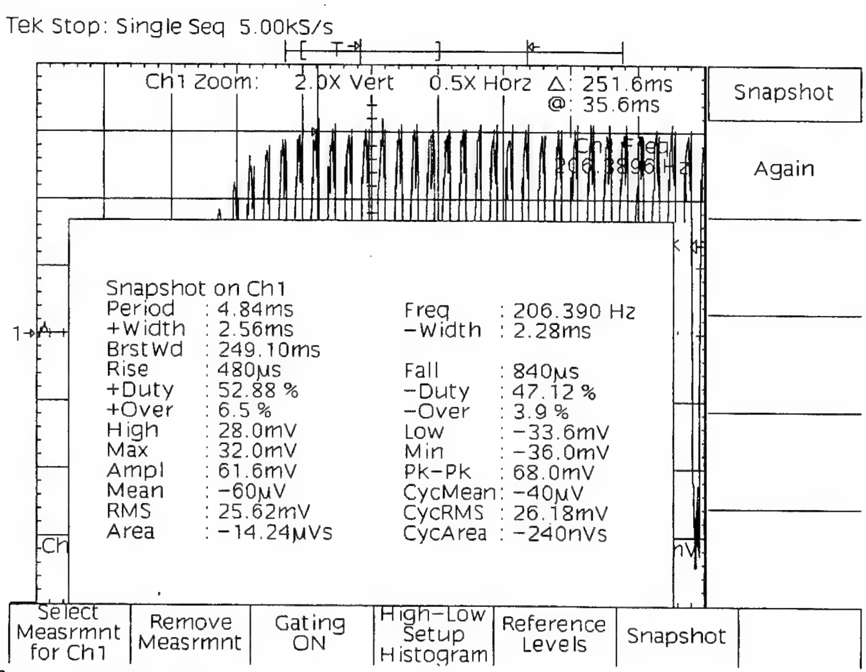

b) Waveform measurements

Figure 3.1 Open Thermoacoustic Prime Mover Data with Standard 20 Mesh Stack

Standard 20 wire mesh stack (16 mil wire, 21 screens), starting ΔT 181 °C, atmospheric pressure

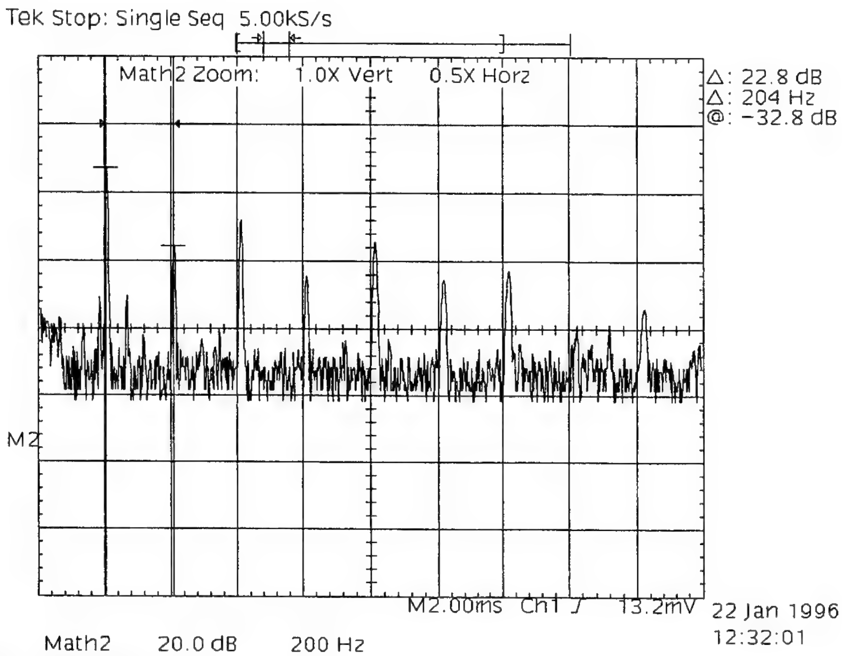

c) Fast Fourier Transform

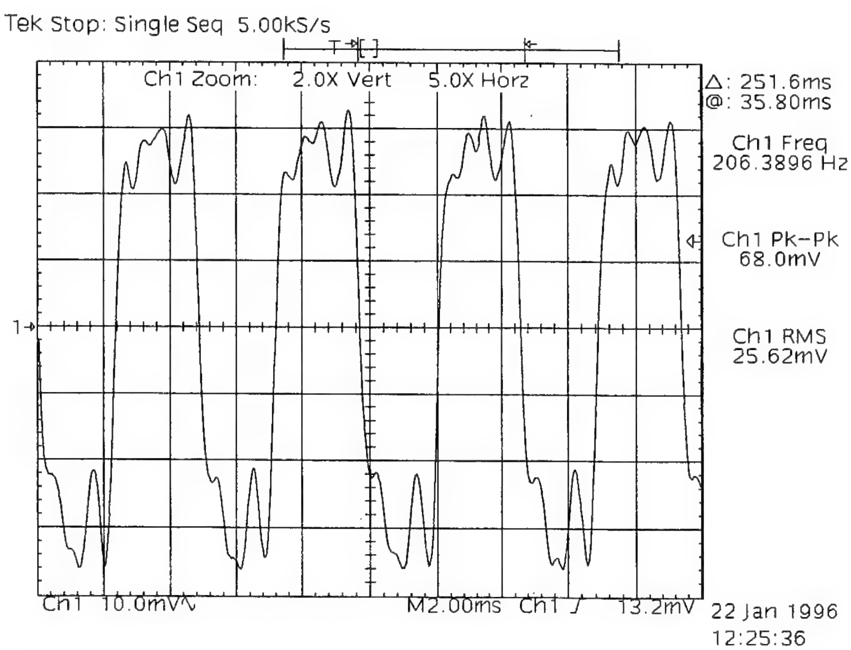

d)Waveform

Figure 3.1 Open Thermoacoustic Prime Mover Data with Standard 20 Mesh Stack (continued)

Polyester spiral roll stack (3 mil film,25 mil spacing) starting ΔT 181 °C, atmospheric pressure

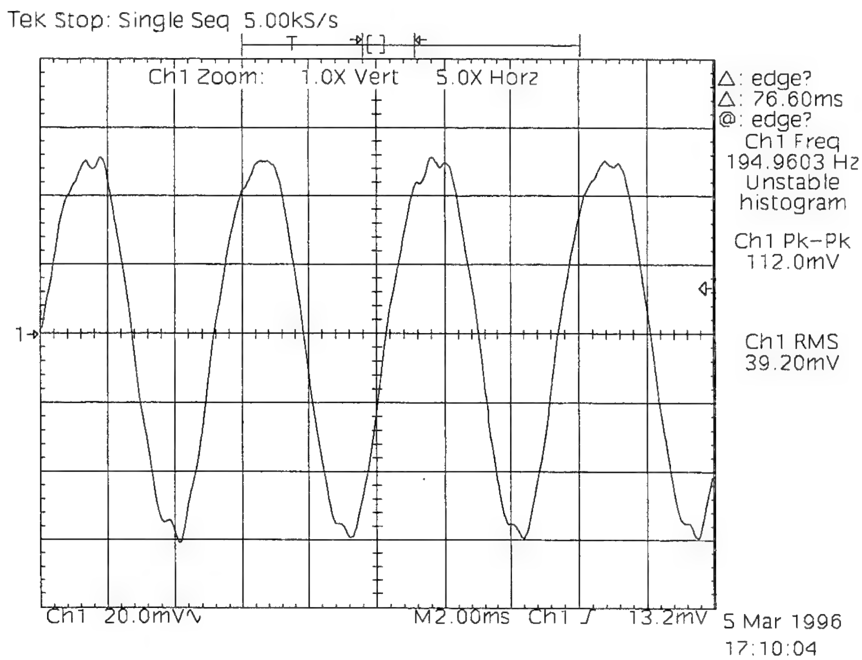

a) Polyester spiral roll stack waveform

Bolting 10 wire mesh stack (10 mil wire, 32 screens), starting ΔT 180 °C, atmospheric pressure

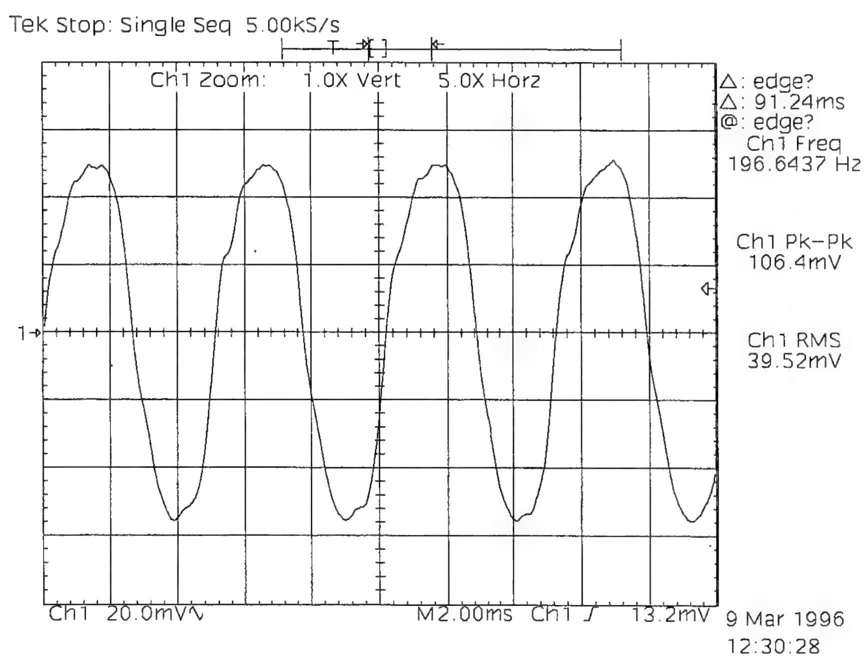

b) Bolting 10 wire mesh stack waveform

Figure 3.2 Open Thermoacoustic Prime Mover waveforms for Poly & Bolting 10

Stack	Porosity	Amplitude	Start T_{Hot}	Start T_{Cold}	Start ΔT	Shutoff ΔT	Frequency	Wire Diameter	Screens	Spacers
Abbreviation	%	mV_{RMS}	°C	°C	°C	°C	Hz	mil	No.	No. / mil
Poly.a	78.2	34.72	11	-158	169	66	190.448			
Poly.b	78.2	34.8	13	-158	171	66	196.079			
Poly.c	78.2	39.2	10	-170	180	77	194.96			
Poly.d	78.2	42.6	10	-170	180	77	193.219			
Bolt 10.a	92.1	35.32	10	-170	180	96	199.412	10	32	
Bolt 10.b	92.1	39.52	10	-170	180	97	196.644	10	32	
Bolt 16	87.4	33.52	10	-170	180	84	199.03	10	28	
Bolt 18.a	87.3	35.28	14	-160	174	76	201.8395	9	33	
Bolt 18.b	87.3	33.64	10	-167	177	77	199.297	9	33	
Bolt 18.c	87.3	33.48	10	-170	180	82	202.413	9	33	
Bolt 18.d	87.3	32.64	12	-170	182	82	201.327	9	38	
Bolt 18.e	92.7	36.28	10	-175	185	106	194.05	9	12	11 / 35
Bolt 18.f	90.7	34.52	12	-169	181	100	196.137	9	19	8 / 35
Bolt 18.g	90.2	34.92	12	-164	176	87	192.66	9	24	23 / 15
Bolt 20	85.9	26.56	8	-166	174	79	202.265	9	33	
Bolt 24	85.9	28.84	10	-170	180	79	212.336	7.5	43	
Bolt 28	83.5	26.6	12	-168	180	76	210.312	7.5	40	
Std 12.a	78.3	32.4	10	-170	180	95	200.146	22.5	14	
Std 12.b	78.3	30.28	10	-170	180	95	196.84	22.5	14	
Std 14	80.2	32.92	10	-170	180	92	194.303	18	18	
Std 18.a	76	29.76	14	-168	182	87	205.309	17	17	
Std 18.b	76	25.94	14	-163	177	84	202.974	17	17	
Std 20	74.9	25.62	11	-170	181	85	206.3896	16	21	
Std 24	73.6	22.38	14	-167	181	85	210.8124	14	24	

Table 3.1 Open Thermoacoustic Prime Mover Data

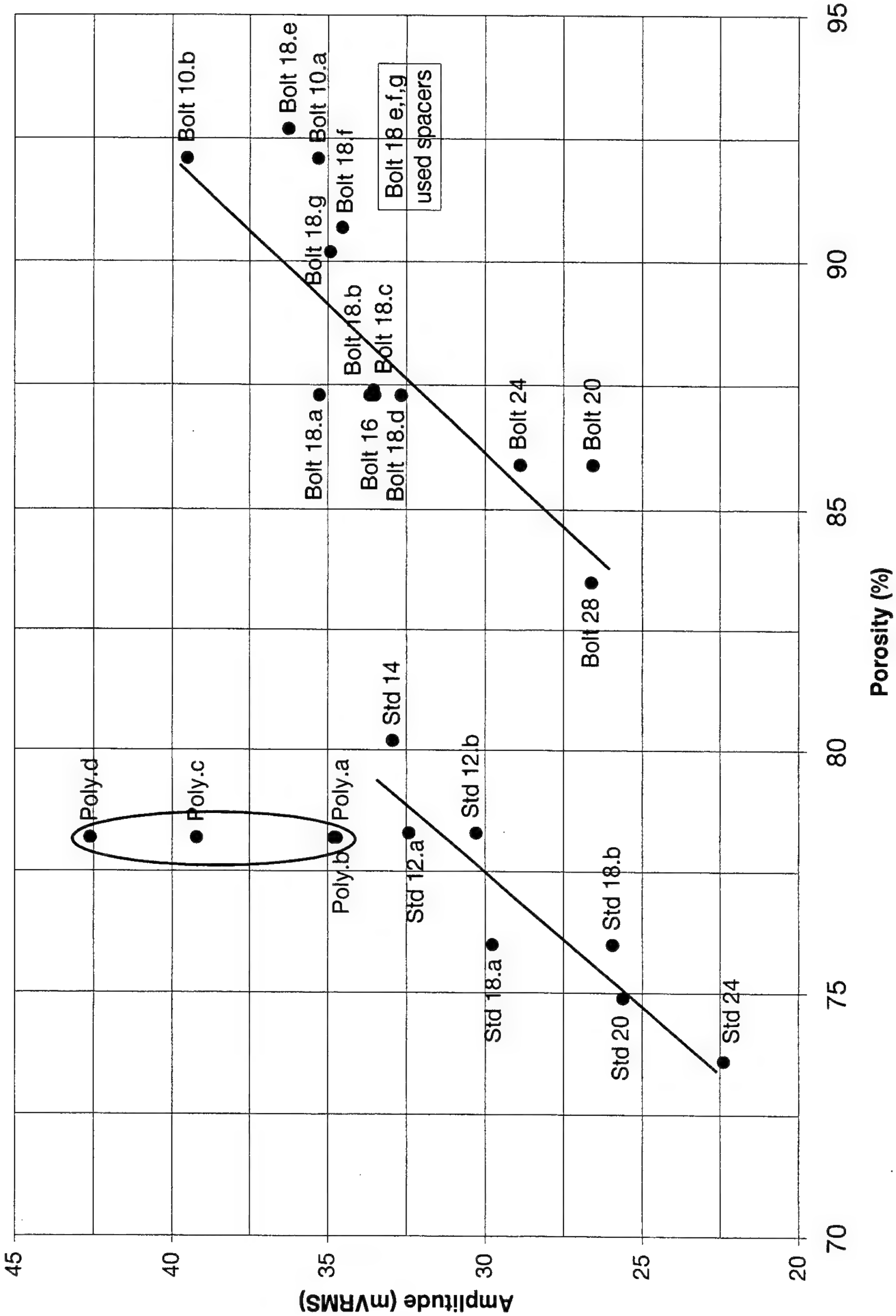

Figure 3.3 Open Prime Mover Amplitude vs Porosity

Plunger	CHXC	CHXW	HHXC	HHXW	TRatio	HTube	HHXave	Pm	Pm	Po/Pm	Freq	Heater	Leak	Q_{hot}	Eff_{Quasi}
cm	°C	°C	°C	°C	°K/°K	°C	°C	psia	kPa	%RMS	Hz	W	W	W	$(kPa/Hz)^{1/2}/W$
Stack: Polyester Spiral Rolled Parallel Plate; Plunger to stack distance: Fixed; Pressure: Variable															
3.94	-161.4	-171.9	1.2	17.2	2.7	28.6	9.2	12.50	86.20	21.78	177.13	166.0	15.0	151.0	0.87
3.94	-164.4	-172.3	3.6	18.8	2.7	29.0	11.2	11.01	75.89	22.07	177.28	153.5	15.0	138.5	0.92
3.94	-166.6	-173.1	5.8	20.8	2.8	29.6	13.3	9.50	65.50	22.32	177.46	143.8	15.0	128.8	0.94
3.94	-169.4	-173.6	12.5	25.0	2.9	30.9	18.8	7.25	49.96	22.48	178.02	120.2	15.0	105.2	1.02
3.94	-172.9	-175.9	17.0	26.8	3.0	31.4	21.9	6.01	41.41	22.40	178.45	104.3	15.0	89.3	1.08
3.94	-177.3	-180.0	25.6	30.9	3.2	32.7	28.3	4.01	27.63	21.38	179.98	70.4	15.0	55.4	1.29
3.94	-181.5	-183.0	30.1	33.0	3.4	33.5	31.6	3.00	20.69	19.95	181.01	50.8	15.0	35.8	1.50
3.94	-187.8	-188.0	34.0	34.8	3.6	34.0	34.4	2.01	13.85	15.76	182.56	30.5	15.0	15.5	1.76
3.94	-190.0	-190.2	34.9	35.3	3.7	34.2	35.1	1.58	10.91	9.83	183.69	20.4	15.0	5.4	1.74
3.94	-189.7	-190.4	35.6	35.8	3.7	34.4	35.7	1.30	8.97	0.09		14.5	15.0	0.0	
Stack: Bolt 10 Mesh; Plunger to stack distance: Fixed; Pressure: Variable															
3.92	-191.1	-191.5	34.7	34.7	3.8	33.1	34.7	0.95	6.58	0.09		16.1	16.5	0.0	
3.92	-190.7	-190.9	34.0	34.2	3.7	33.4	34.1	1.28	8.81	7.39	181.47	20.3	16.5	3.8	1.26
3.92	-190.5	-190.3	33.1	33.4	3.7	33.4	33.2	1.58	10.91	10.57	181.18	21.3	16.5	4.8	2.28
3.92	-190.0	-189.4	31.5	32.0	3.7	33.1	31.7	2.01	13.83	13.38	180.85	26.0	16.5	9.5	2.07
3.92	-187.8	-186.7	28.1	29.5	3.5	32.6	28.8	3.01	20.73	17.04	180.08	37.0	16.5	20.5	1.91
3.92	-185.6	-184.4	24.4	27.5	3.4	31.7	25.9	4.00	27.61	18.79	179.56	49.3	16.5	32.8	1.69
3.92	-179.9	-181.6	17.1	23.4	3.2	30.2	20.2	6.00	41.38	20.30	178.72	70.2	16.5	53.7	1.47
3.92	-177.4	-180.0	13.5	21.5	3.1	29.0	17.5	7.25	49.99	20.70	178.30	82.4	16.5	65.9	1.37
3.92	-173.7	-178.7	7.6	18.2	3.0	27.3	12.9	9.50	65.52	20.87	177.90	100.6	16.5	84.1	1.25
3.92	-172.2	-177.9	4.6	16.7	2.9	26.2	10.7	11.00	75.85	20.82	177.75	111.5	16.5	95.0	1.19
3.92	-170.5	-177.0	2.0	15.3	2.8	25.4	8.7	12.50	86.16	20.66	177.63	121.0	16.5	104.5	1.14
Stack: Bolt 16 Mesh; Plunger to stack distance: Fixed; Pressure: Variable															
3.94	-175.6	-180.2	6.4	18.1	3.0	26.0	12.2	12.50	86.17	19.08	179.73	106.6	17.5	89.1	1.13
3.94	-177.5	-181.6	8.9	19.7	3.1	26.5	14.3	11.00	75.85	19.03	179.96	94.7	17.5	77.2	1.22
3.94	-179.7	-183.0	12.2	21.6	3.2	27.5	16.9	9.51	65.54	18.86	180.26	82.0	17.5	64.5	1.33
3.94	-183.3	-185.7	17.4	24.3	3.3	28.6	20.8	7.25	49.98	18.21	180.94	64.8	17.5	47.3	1.47
3.94	-189.0	-189.9	26.7	28.8	3.6	30.3	27.8	4.01	27.63	15.06	182.13	36.3	17.5	18.8	1.87
3.94	-190.3	-191.0	29.7	30.5	3.7	30.9	30.1	3.01	20.72	12.61	182.69	28.1	17.5	10.6	2.02
3.94	-191.0	-191.6	32.1	32.1	3.7	31.4	32.1	1.99	13.73	7.67	183.31	20.4	17.5	2.9	2.22
3.94	-191.5	-191.8	32.7	32.7	3.8	31.6	32.7	1.36	9.36	0.06		17.6	17.5	0.1	

Table 3.2 Sealed Thermoacoustic Prime Mover Data

Stack: Polyester Spiral Rolled Parallel Plate; Plunger to stack distance: Fixed; Pressure: Variable															
Plunger	CHXC	CHXW	HHXC	HHXW	TRatio	HTube	HHXave	Pm	Pm	Po/Pm	Freq	Heater	Leak	Q_{hot}	Eff_{Quasi}
cm	°C	°C	°C	°C	°K/°K	°C	°C	psia	kPa	%RMS	Hz	W	W	W	$(kPa/Hz)^{1/2}/W$
8.15	-144.3	-161.0	-18.5	8.5	2.2	25.4	-5.0	11.00	75.87	18.96	164.56	236.8	14.5	222.3	0.44
8.15	-146.8	-162.6	-15.2	10.7	2.3	26.2	-2.3	9.50	65.48	19.45	164.97	224.8	14.5	210.3	0.45
8.15	-153.6	-167.2	-9.6	14.1	2.4	27.6	2.2	7.25	49.99	20.39	165.88	200.2	14.5	185.7	0.49
8.15	-160.4	-170.9	1.6	19.9	2.6	29.9	10.8	5.00	34.46	20.74	168.30	155.4	14.5	140.9	0.55
8.15	-166.4	-174.4	8.5	23.7	2.8	31.3	16.1	4.00	27.60	20.51	170.06	127.0	14.5	112.5	0.60
8.15	-173.3	-178.0	17.8	28.4	3.0	32.6	23.1	3.01	20.73	19.23	172.52	91.2	14.5	76.7	0.67
8.15	-177.2	-180.3	23.4	31.1	3.2	33.3	27.3	2.50	17.26	17.73	173.94	71.1	14.5	56.6	0.70
8.15	-181.4	-183.4	29.7	34.0	3.4	34.0	31.8	2.01	13.82	15.06	175.54	45.1	14.5	30.6	0.83
8.15	-186.0	-187.2	34.7	35.7	3.6	34.3	35.2	1.58	10.93	10.24	176.54	26.3	14.5	11.8	0.88
8.15	-190.2	-191.0	35.5	35.8	3.7	34.4	35.7	1.32	9.12	0.09		14.1	14.5	0.0	
Stack: Bolt 10 Mesh; Plunger to stack distance: Fixed; Pressure: Variable															
8.15	-191.1	-191.6	32.9	33.1	3.7	31.8	33.0	1.00	6.89	0.10		14.0	15.0	0.0	
8.15	-186.2	-187.0	28.5	30.0	3.5	30.52	29.3	2.00	13.81	11.50	173.60	32.1	15.0	17.1	0.87
8.15	-183.6	-185.3	25.7	28.8	3.4	30.08	27.2	2.50	17.24	13.64	172.90	42.8	15.0	27.8	0.84
8.15	-181.0	-184.0	22.2	26.9	3.3	29.46	24.5	3.00	20.69	15.00	172.32	52.4	15.0	37.4	0.83
8.15	-176.7	-181.5	15.8	23.4	3.1	28.25	19.6	4.00	27.61	16.50	171.41	73.2	15.0	58.2	0.75
8.15	-170.4	-176.7	13.4	23.7	2.9	29.11	18.5	5.00	34.46	16.93	170.89	88.0	15.0	73.0	0.70
8.15	-165.7	-175.2	0.9	17.3	2.8	25.82	9.1	7.26	50.03	17.85	168.67	129.4	15.0	114.4	0.61
8.15	-160.5	-172.1	-7.4	12.8	2.6	23.36	2.7	9.51	65.54	17.65	167.40	152.5	15.0	137.5	0.57
8.15	-158.0	-170.4	-13.0	9.1	2.5	20.13	-2.0	11.00	75.86	17.28	166.73	167.3	15.0	152.3	0.53
Stack: Bolt 16 Mesh; Plunger to stack distance: Fixed; Pressure: Variable															
8.15	-165.9	-175.0	0.5	18.1	2.8	26.7	9.3	10.00	68.93	15.26	170.17	128.9	16.0	112.9	0.52
8.15	-172.5	-178.9	9.9	23.4	3.0	29.2	16.7	7.25	50.00	14.96	172.06	95.9	16.0	79.9	0.60
8.15	-180.1	-183.2	19.9	28.4	3.3	30.9	24.1	5.00	34.47	13.83	173.87	64.8	16.0	48.8	0.70
8.15	-183.8	-185.4	24.6	30.4	3.4	31.8	27.5	4.00	27.60	12.66	174.66	50.2	16.0	34.2	0.74
8.15	-187.2	-188.1	29.5	32.4	3.6	32.5	30.9	3.00	20.69	10.55	175.40	35.1	16.0	19.1	0.80
8.15	-189.0	-189.7	32.0	33.5	3.7	33.0	32.7	2.50	17.25	8.80	175.76	27.4	16.0	11.4	0.85
8.15	-190.8	-191.3	34.0	34.3	3.7	33.4	34.1	2.00	13.81	6.11	175.89	20.7	16.0	4.7	0.89
8.15	-191.4	-191.8	34.9	34.9	3.8	33.6	34.9	1.59	10.93	2.80	176.19	17.1	16.0	1.1	

Table 3.2 Sealed Thermoacoustic Prime Mover Data (continued)

Stack: Polyester Spiral Rolled Parallel Plate; Plunger to stack distance: Fixed; Pressure: Variable															
Plunger	CHXC	CHXW	HHXC	HHXW	TRatio	HTube	HHXave	Pm	Pm	Po/Pm	Freq	Heater	Leak	Q_{hot}	Eff_{Quasi}
cm	°C	°C	°C	°C	°K/°K	°C	°C	psia	kPa	%RMS	Hz	W	W	W	$(kPa/Hz)^{1/2}/W$
10.69	-190.2	-190.9	35.3	35.6	3.7	34.4	35.5	1.47	10.11	0.08		15.0	15.0	0.0	
10.69	-186.8	-187.9	34.3	35.2	3.6	34.1	34.8	1.58	10.91	7.57	172.30	24.4	15.0	9.4	0.61
10.69	-181.6	-184.0	27.9	32.5	3.4	33.4	30.2	2.00	13.81	12.75	170.86	49.8	15.0	34.8	0.53
10.69	-177.1	-181.1	21.6	29.7	3.2	33.0	25.7	2.49	17.20	15.39	168.98	74.1	15.0	59.1	0.51
10.69	-172.3	-178.5	15.6	26.8	3.0	32.7	21.2	3.01	20.74	16.77	167.23	98.7	15.0	83.7	0.47
10.69	-164.9	-174.1	5.5	21.4	2.8	31.0	13.5	4.00	27.55	17.75	164.51	136.1	15.0	121.1	0.42
10.69	-159.4	-171.5	-2.4	17.2	2.6	29.3	7.4	4.99	34.43	18.04	162.46	167.6	15.0	152.6	0.39
10.69	-150.6	-165.7	-13.2	11.7	2.4	26.8	-0.7	7.25	49.99	17.59	159.90	212.1	15.0	197.1	0.35
10.69	-144.0	-161.2	-19.2	8.1	2.2	25.2	-5.6	9.50	65.50	16.82	158.72	237.0	15.0	222.0	0.33
10.69	-143.3	-161.2	-24.0	5.5	2.2	24.0	-9.2	11.01	75.88	16.56	158.16	254.0	15.0	239.0	0.32
Stack: Bolt 10 Mesh; Plunger to stack distance: Fixed; Pressure: Variable															
10.69	-156.0	-169.2	-14.5	9.6	2.5	20.49	-2.5	11.01	75.89	14.50	161.10	175.4	17.5	157.9	0.36
10.69	-158.7	-171.1	-9.9	12.3	2.5	22.041	1.2	9.50	65.48	14.74	162.01	162.2	17.5	144.7	0.38
10.69	-164.3	-174.4	-3.1	14.8	2.7	23.626	5.9	7.25	50.01	14.77	163.80	131.4	17.5	113.9	0.42
10.69	-171.8	-178.8	8.8	20.7	2.9	26.313	14.8	5.00	34.50	14.42	166.30	96.3	17.5	78.8	0.48
10.69	-176.3	-181.2	15.3	23.9	3.1	27.764	19.6	4.00	27.55	13.78	167.64	76.6	17.5	59.1	0.52
10.69	-180.9	-183.9	22.3	27.4	3.3	29.215	24.9	3.00	20.70	12.36	169.17	54.0	17.5	36.5	0.58
10.69	-183.6	-185.5	26.1	29.5	3.4	30.145	27.8	2.50	17.26	11.07	169.97	42.5	17.5	25.0	0.62
10.69	-186.3	-187.3	31.1	32.8	3.5	32.191	32.0	2.00	13.81	9.08	170.77	33.3	17.5	15.8	0.59
10.69	-189.1	-189.5	33.4	33.9	3.7	33.091	33.6	1.58	10.92	6.22	170.97	23.9	17.5	6.4	0.61
10.69	-190.7	-191.1	34.5	34.6	3.7	33.517	34.6	1.28	8.79	3.06	170.20	18.5	17.5	1.0	
10.69	-191.1	-191.5	35.1	35.2	3.8	33.8	35.2	1.13	7.76	0.09		16.5	17.5	0.0	
Stack: Bolt 16 Mesh; Plunger to stack distance: Fixed; Pressure: Variable															
10.69	-188.9	-189.3	34.0	34.0	3.7	33.0	34.0	1.58	10.90	1.61	167.81	12.7	14.0	0.0	
10.69	-189.3	-189.9	32.8	33.2	3.7	32.7	33.0	2.07	14.25	4.88	169.73	20.0	14.0	6.0	0.46
10.69	-187.3	-188.1	31.1	32.7	3.6	32.6	31.9	2.54	17.49	6.94	169.55	23.6	14.0	9.6	0.64
10.69	-185.5	-186.6	29.2	32.2	3.5	32.5	30.7	3.01	20.73	8.45	169.23	31.2	14.0	17.2	0.58
10.69	-182.7	-185.2	23.4	29.5	3.4	31.3	26.5	4.02	27.70	10.55	168.17	53.0	14.0	39.0	0.46
10.69	-178.8	-182.8	18.6	27.3	3.2	30.7	23.0	5.00	34.49	11.44	167.56	66.4	14.0	52.4	0.45
10.69	-171.8	-178.8	8.4	22.3	3.0	28.7	15.3	7.25	50.01	12.35	166.28	97.9	14.0	83.9	0.40
10.69	-164.1	-173.6	-0.7	17.4	2.7	26.4	8.4	10.01	68.98	12.39	164.64	129.3	14.0	115.3	0.34

Table 3.2 Sealed Thermoacoustic Prime Mover Data (continued)

Stack: Polyester Spiral Rolled Parallel Plate; Plunger to stack distance: Variable; Pressure: 50 kPa															
Plunger	CHXC	CHXW	HHXC	HHXW	TRatio	HTube	HHXave	Pm	Pm	Po/Pm	Freq	Heater	Leak	Q_{hot}	Eff_{Quasi}
cm	°C	°C	°C	°C	°K/°K	°C	°C	psia	kPa	%RMS	Hz	W	W	W	$(kPa/Hz)^{1/2}/W$
3.95	-170.6	-174.8	11.9	24.4	2.9	30.8	18.2	7.26	50.03	22.58	177.88	121.1	15.0	106.1	1.02
6.37	-155.8	-167.9	-2.9	17.3	2.5	28.9	7.2	7.26	50.02	22.13	170.57	177.9	15.0	162.9	0.65
8.91	-151.8	-166.4	-11.3	13.0	2.4	27.5	0.9	7.25	50.01	19.52	164.11	204.4	15.0	189.4	0.44
11.47	-151.2	-167.0	-15.1	10.6	2.4	26.3	-2.3	7.26	50.02	16.91	158.33	218.2	15.0	203.2	0.32
14.01	-150.0	-166.1	-15.8	10.1	2.3	25.8	-2.9	7.25	49.99	14.48	153.41	218.0	15.0	203.0	0.24
16.55	-150.9	-167.0	-16.0	9.9	2.4	25.4	-3.1	7.25	49.98	12.58	148.92	216.5	15.0	201.5	0.18
18.91	-151.8	-168.0	-15.6	10.1	2.4	25.4	-2.7	7.25	49.99	11.14	145.25	215.0	15.0	200.0	0.15
Stack: Bolt 10 Mesh; Plunger to stack distance: Variable; Pressure: 50 kPa															
3.94	-177.4	-180.2	0.0	21.2	3.0	29.2	10.6	7.25	50.00	20.67	178.37	84.1	16.5	67.6	1.34
6.37	-167.4	-175.5	3.6	18.1	2.8	27.8	10.8	7.25	50.02	19.67	172.90	116.7	16.5	100.2	0.83
8.91	-164.9	-174.7	-0.7	16.2	2.7	27.4	7.7	7.25	50.00	16.86	167.59	130.0	16.5	113.5	0.55
11.47	-164.5	-174.6	-2.5	15.6	2.7	27.2	6.5	7.25	50.01	14.12	162.81	136.4	16.5	119.9	0.37
14.01	-165.0	-175.2	0.0	15.8	2.7	27.3	7.9	7.25	50.02	11.88	158.39	133.9	16.5	117.4	0.27
16.55	-165.8	-175.9	-0.6	16.8	2.8	27.5	8.1	7.25	50.01	10.11	154.41	132.4	16.5	115.9	0.20
18.91	-164.5	-174.1	3.5	19.7	2.7	29.8	11.6	7.26	50.04	8.62	151.14	114.7	16.5	98.2	0.17
Stack: Bolt 16 Mesh; Plunger to stack distance: Variable; Pressure: 50 kPa															
4.00	-182.9	-185.6	17.4	24.1	3.3	28.5	20.7	7.25	49.95	18.20	180.86	67.3	15.0	52.3	1.33
5.22	-178.0	-181.7	13.6	22.7	3.1	28.0	18.1	7.25	49.99	17.79	178.41	81.2	15.0	66.2	1.01
7.81	-173.3	-179.7	8.8	21.6	3.0	27.5	15.2	7.26	50.03	15.26	173.41	94.2	15.0	79.2	0.63
10.36	-172.4	-179.6	7.3	20.7	3.0	27.1	14.0	7.25	49.99	12.54	168.69	98.8	15.0	83.8	0.41
12.89	-172.9	-180.0	7.7	20.9	3.0	26.9	14.3	7.25	50.01	10.34	164.39	95.9	15.0	80.9	0.29
18.81	-175.5	-181.8	11.1	22.4	3.1	27.3	16.8	7.25	50.01	6.86	155.82	85.4	15.0	70.4	0.15

Table 3.2 Sealed Thermoacoustic Prime Mover Data (continued)

Polyester spiral roll stack, Plunger position 3.94 cm, Pressure 86.2 kPa

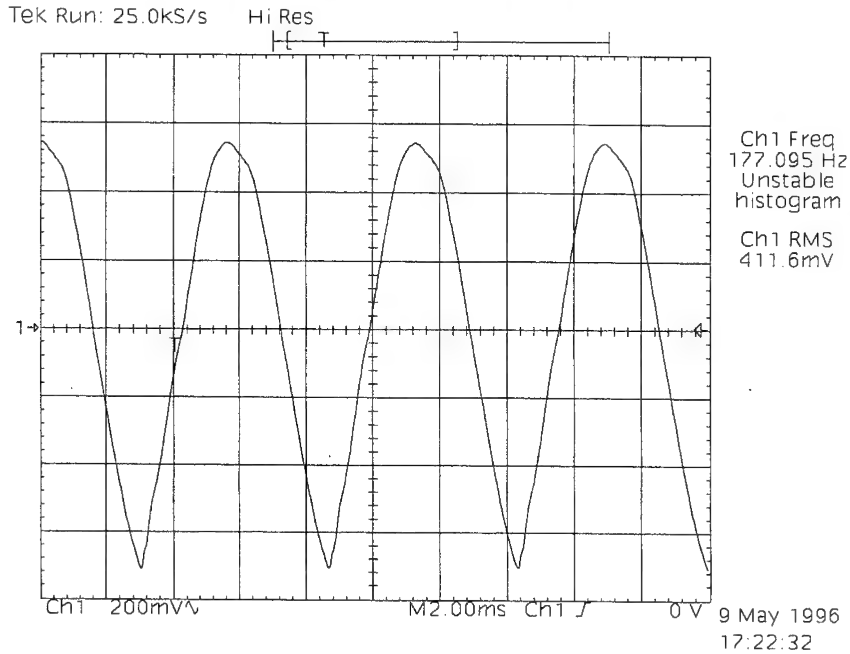

a) Polyester spiral roll stack waveform

Bolting 10 wire mesh stack, Plunger position 3.94 cm, Pressure 86.2 kPa

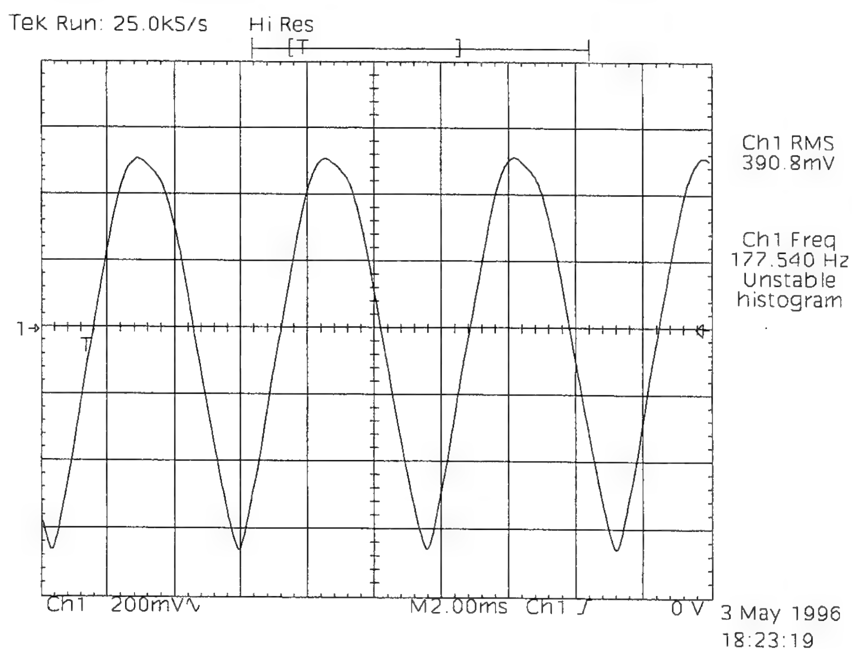

b) Bolting 10 wire mesh stack waveform

Figure 3.4 Sealed Thermoacoustic Prime Mover waveforms for Poly & Bolting 10

Polyester spiral roll stack, Plunger position 8.15 cm,   Pressure 86.2 kPa

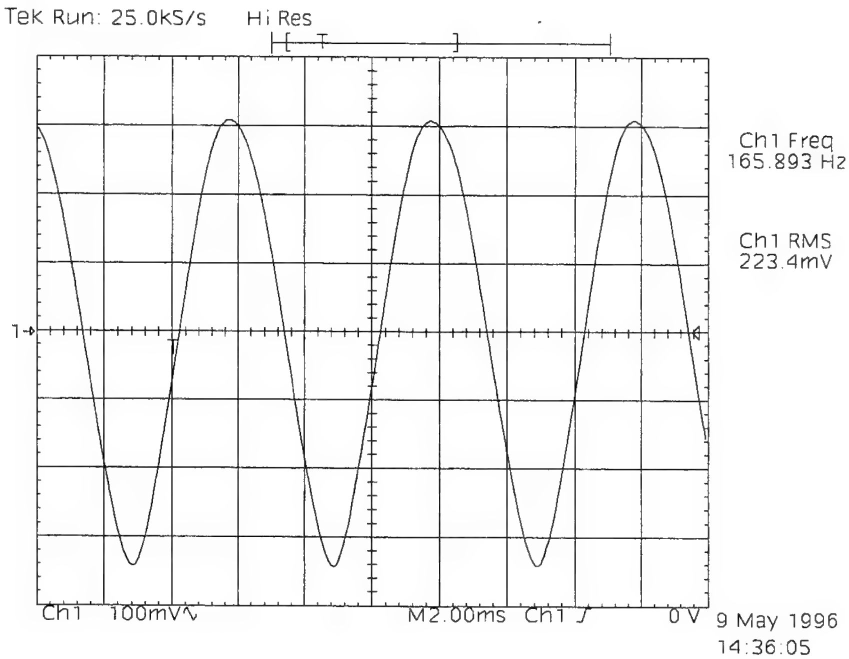

a) Polyester spiral roll stack waveform

Bolting 16 wire mesh stack, Plunger position 7.81 cm,   Pressure 86.2 kPa

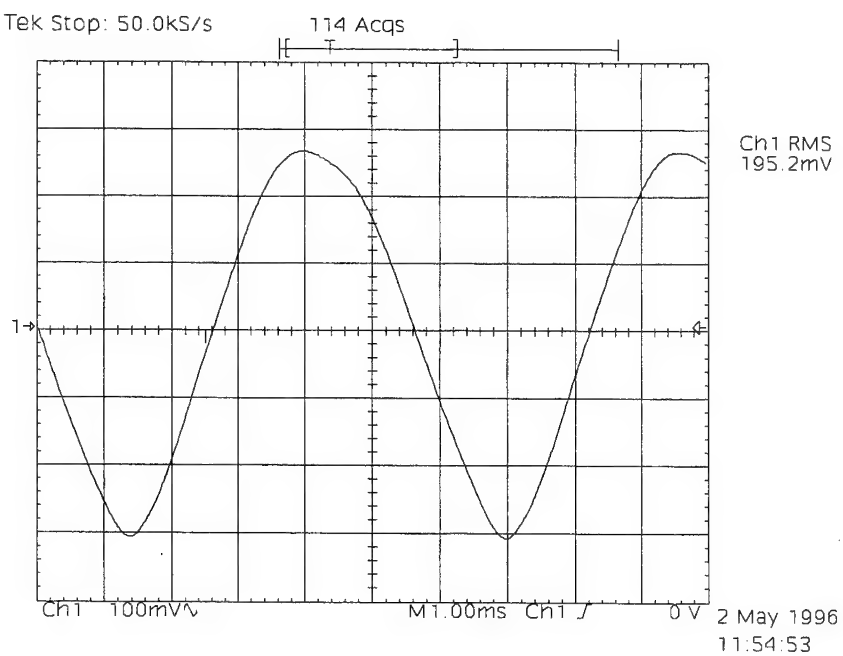

b) Bolting 16 wire mesh stack waveform

Figure 3.5 Sealed Thermoacoustic Prime Mover waveforms for Poly & Bolting 16

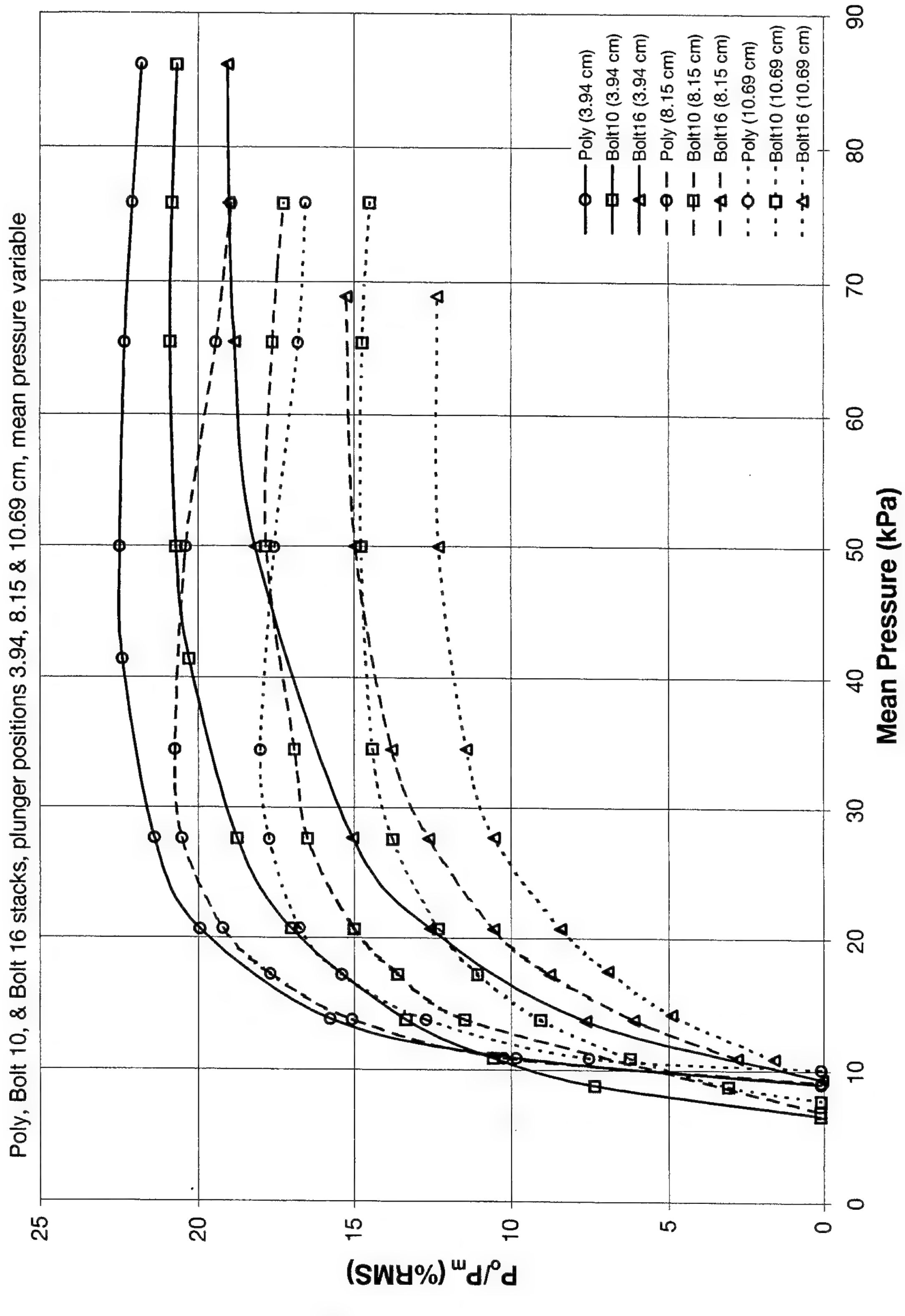

Figure 3.6 Dynamic/Mean Pressure Ratio vs Mean Pressure

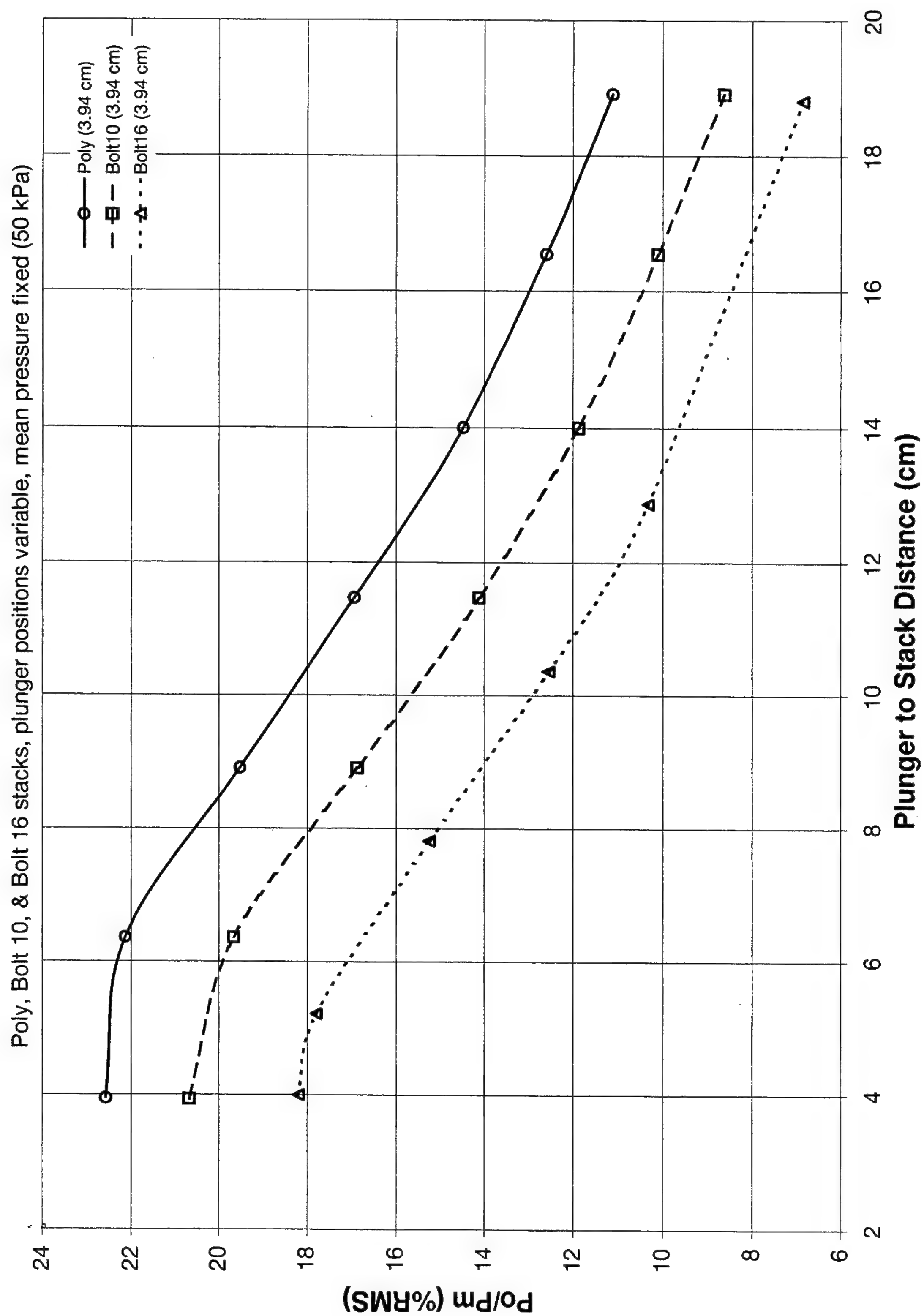

Figure 3.7 Dynamic/Mean Pressure Ratio vs Plunger Position

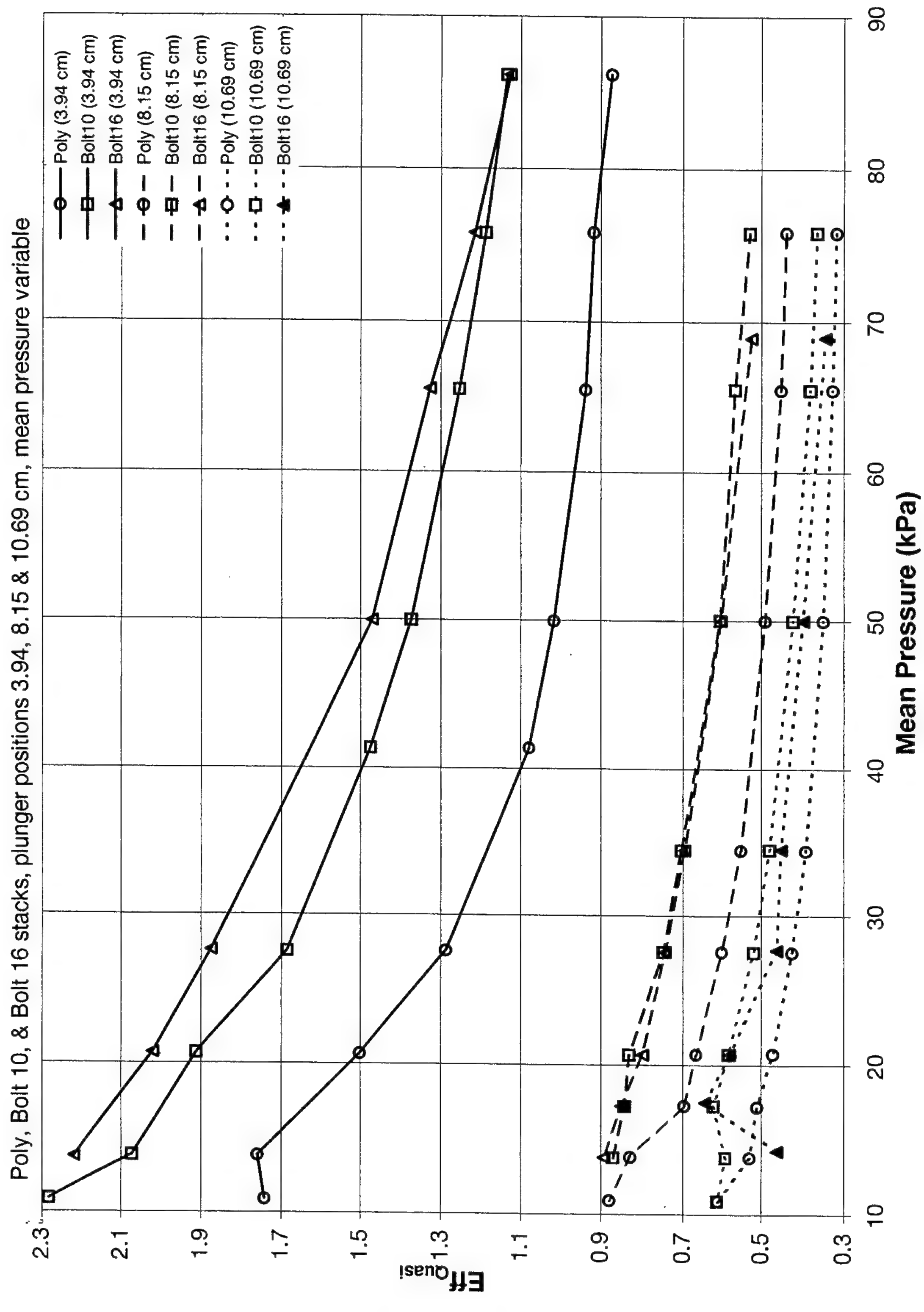

Figure 3.8 Quasi-Efficiency vs Mean Pressure

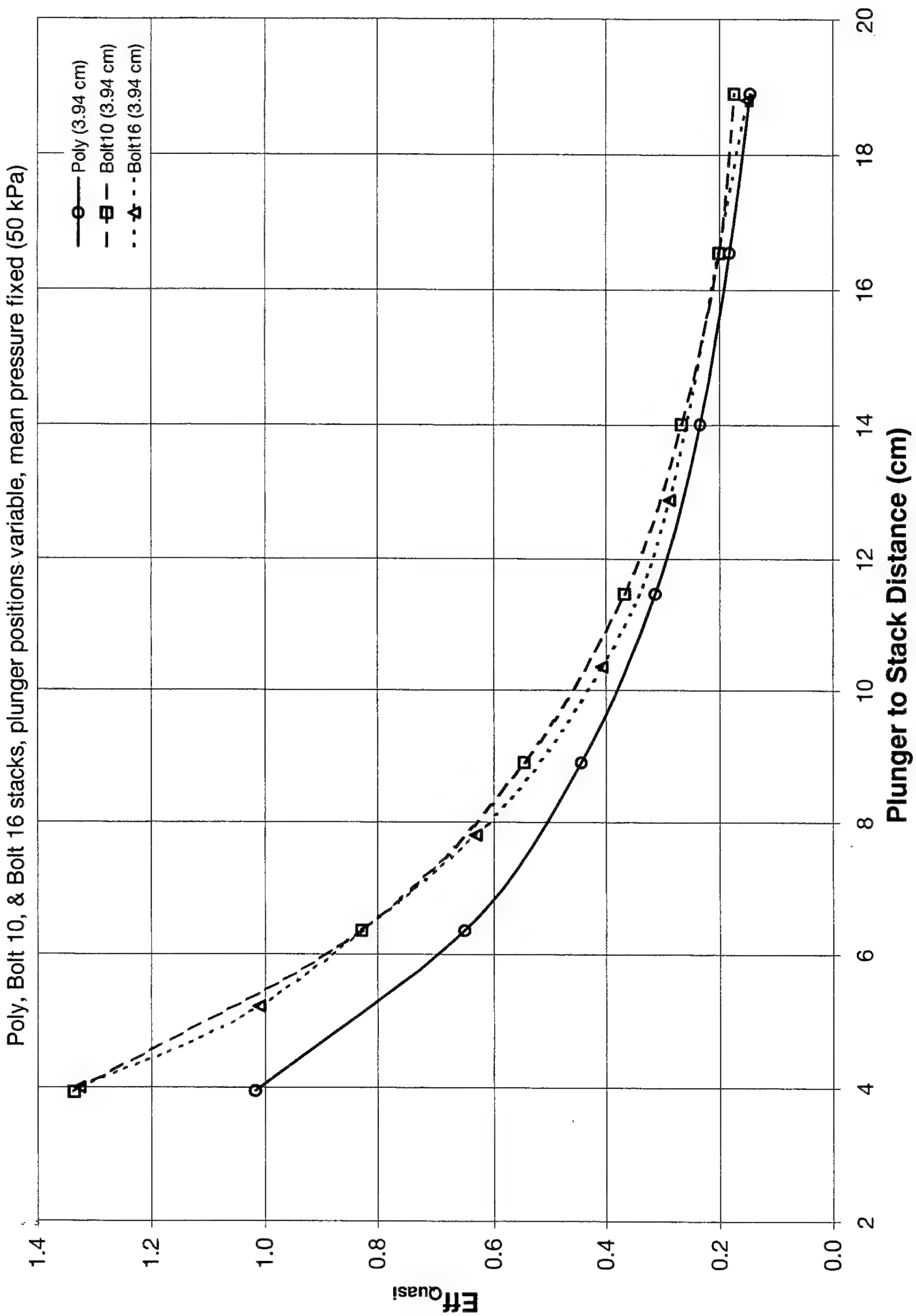

Figure 3.9 Quasi-Efficiency vs Plunger Position

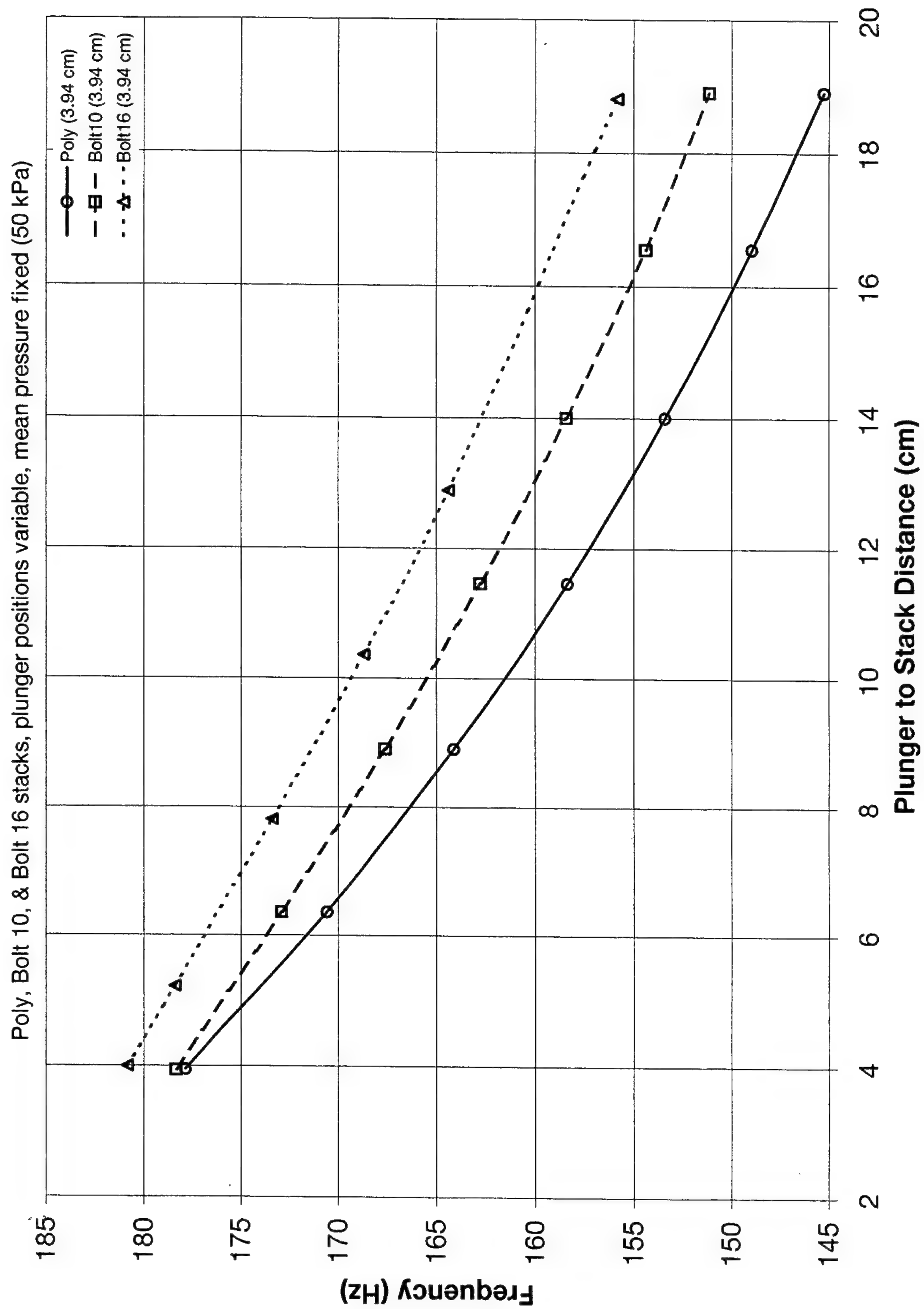

Figure 3.10 Frequency vs Plunger Position

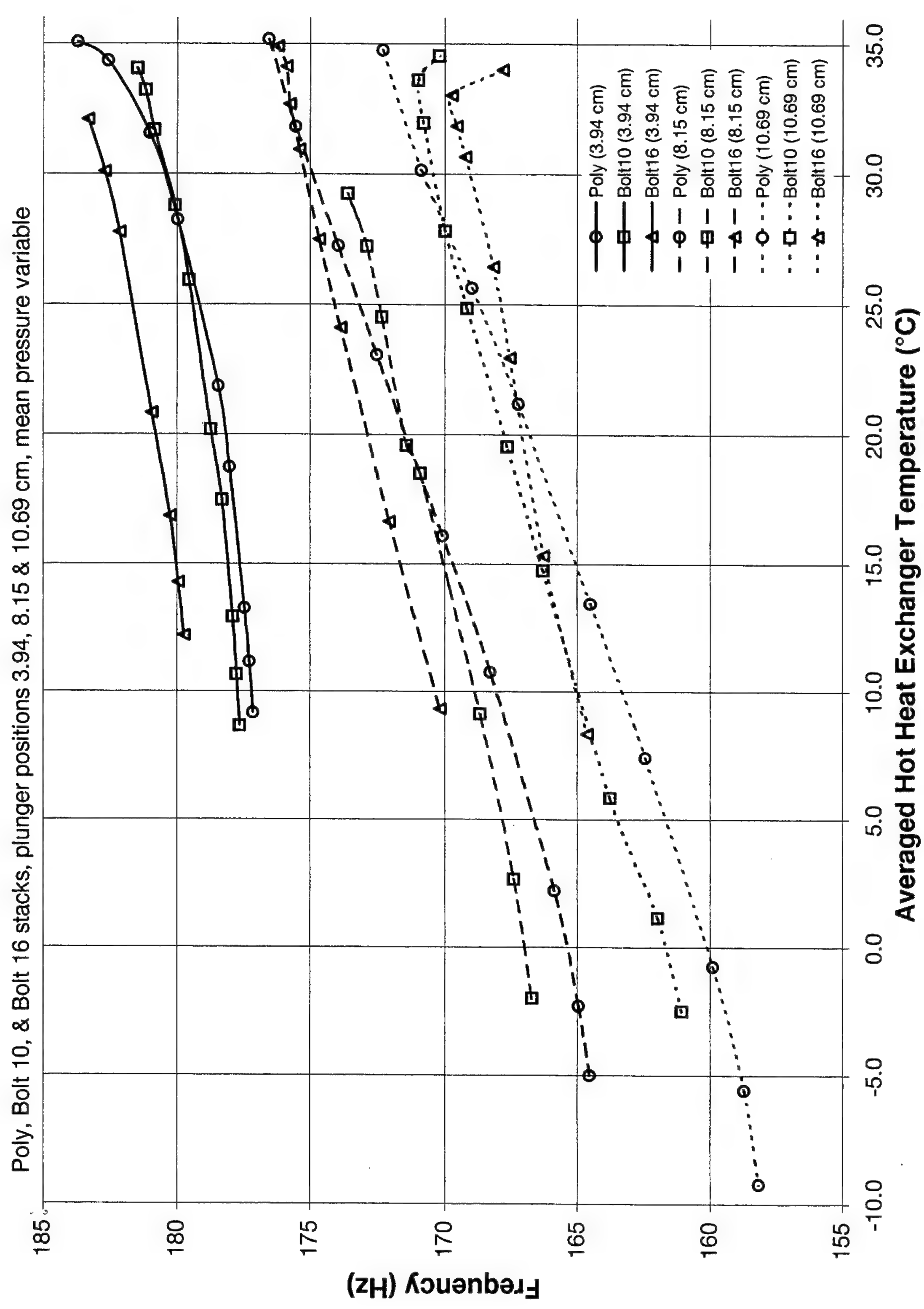

Figure 3.11 Frequency vs Averaged Hot Heat Exchanger Temperature

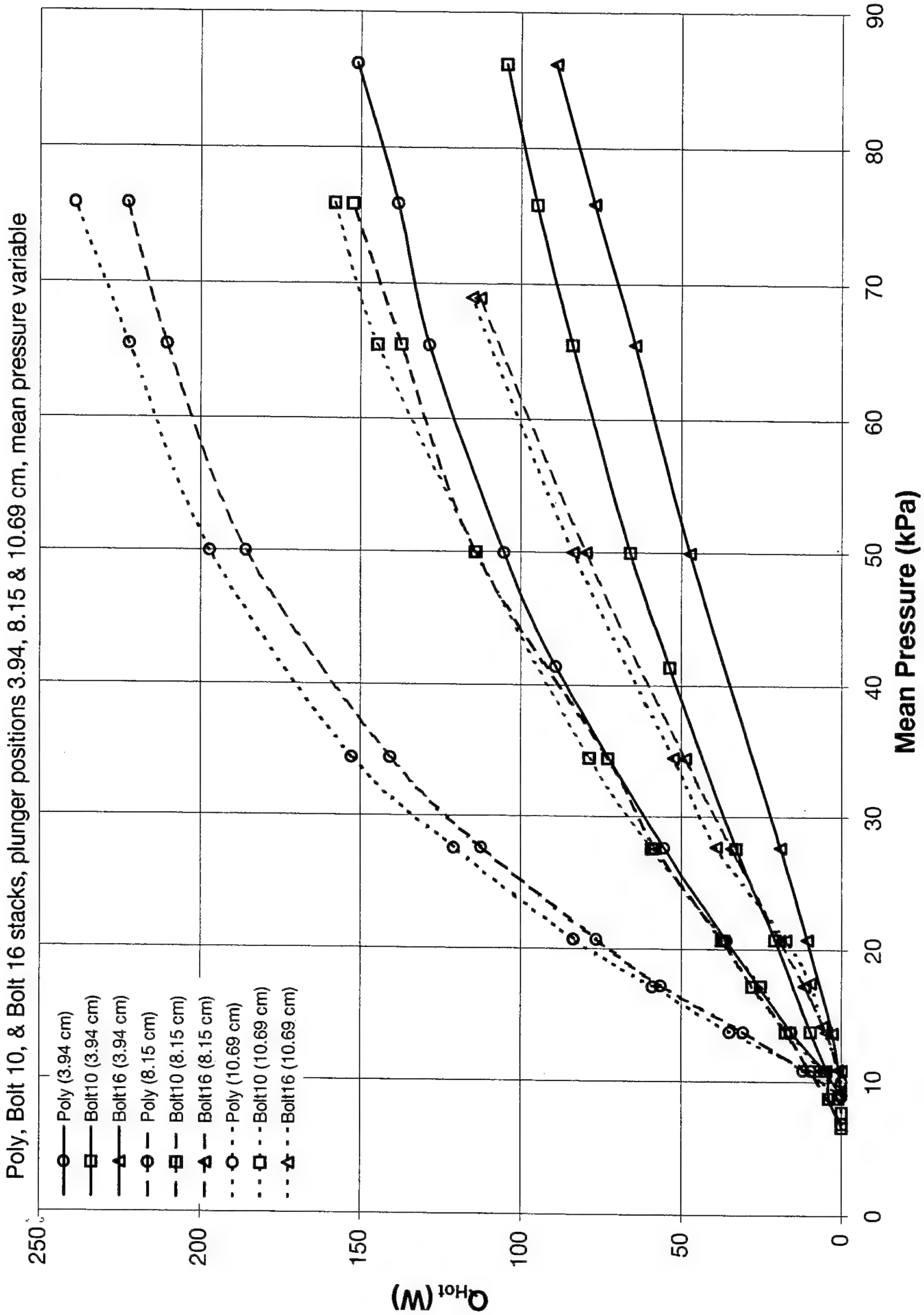

Figure 3.12 Thermoacoustic Heat Input vs Mean Pressure

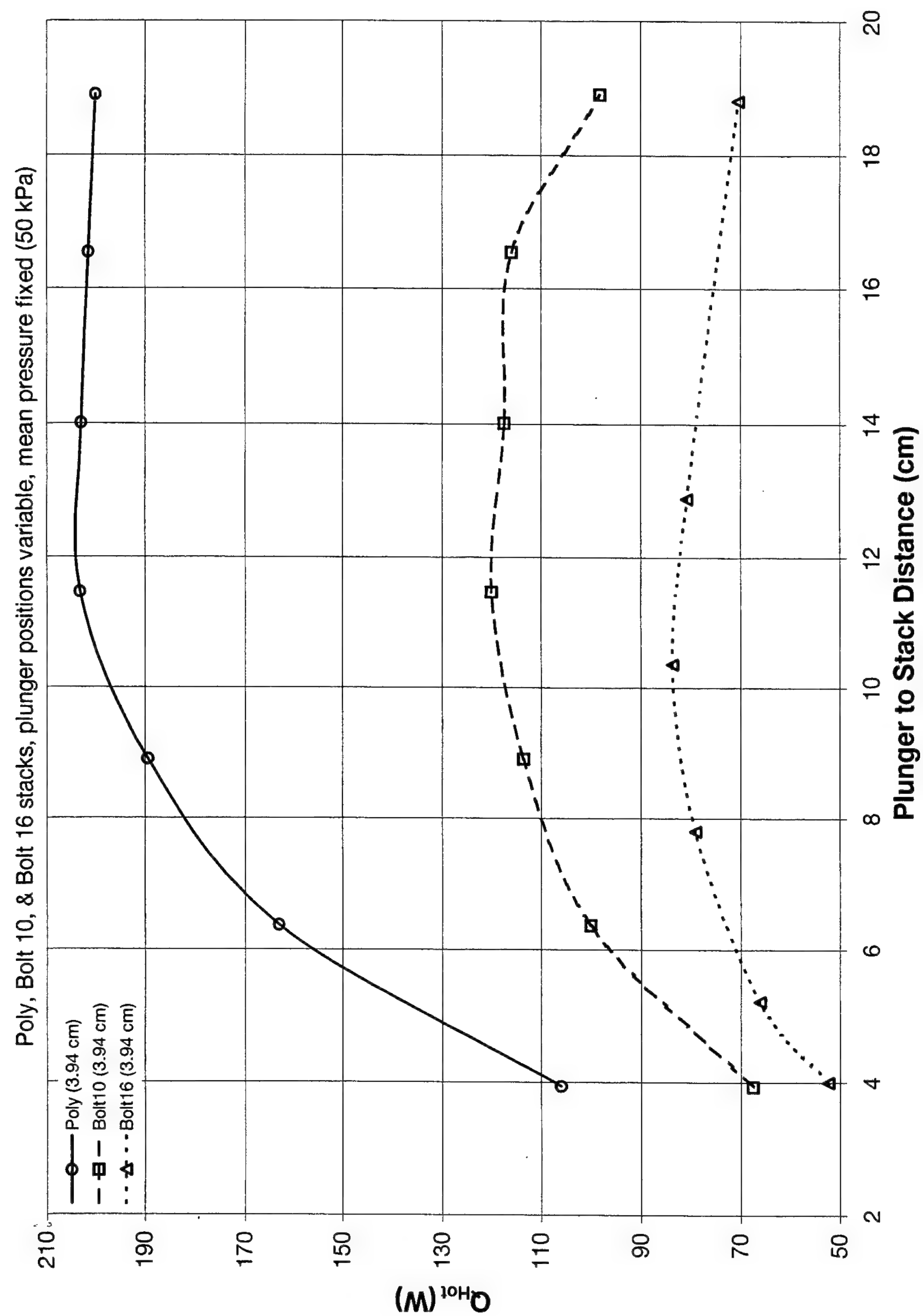

Figure 3.13 Thermoacoustic Heat Input vs Plunger Position

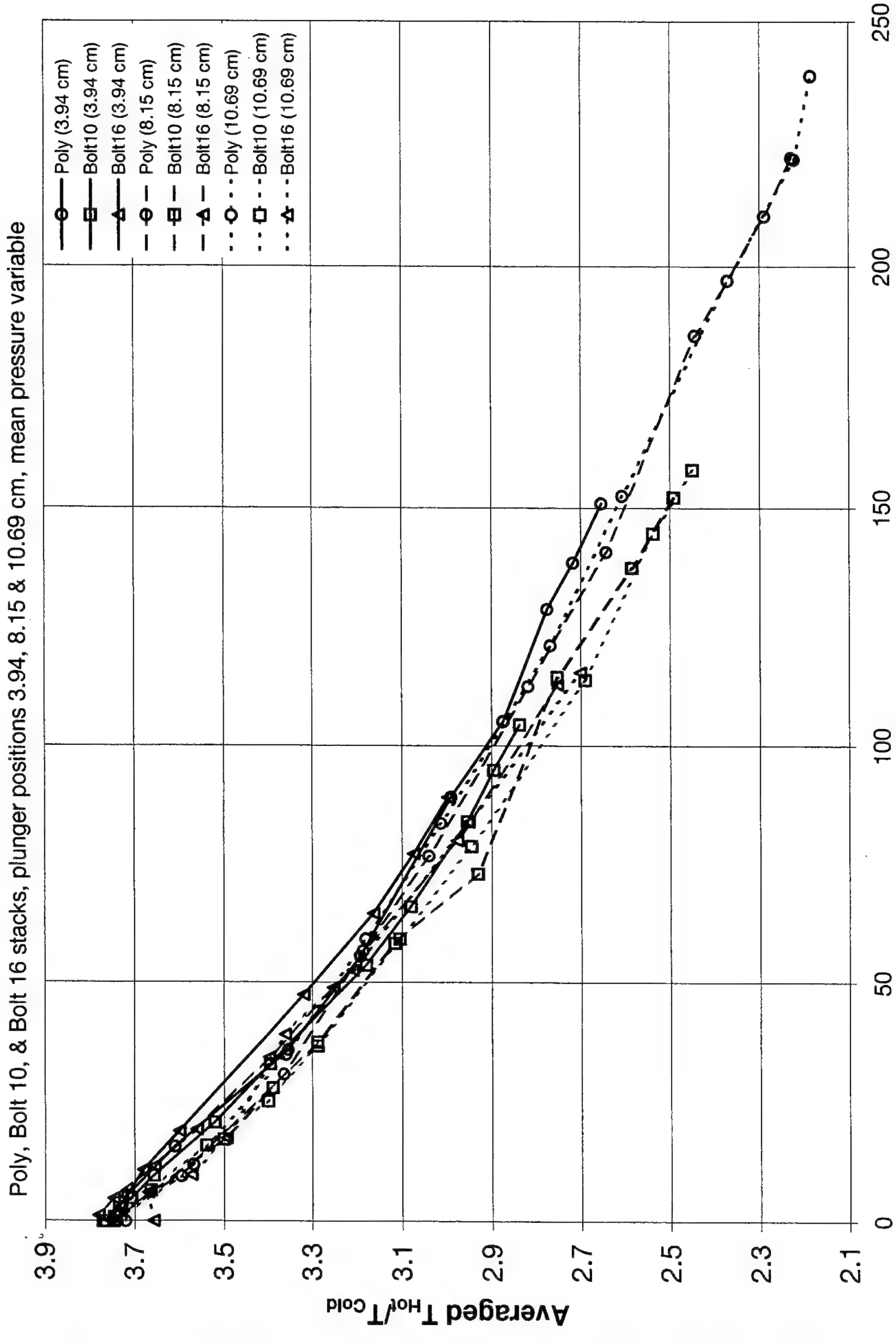

Figure 3.14 Averaged Temperature Ratio vs Thermoacoustic Heat Input

IV. SUMMARY, CONCLUSIONS, AND RECOMMENDATIONS

A. SUMMARY

The goal of this thesis was to investigate the experimental performance of wire mesh screen stacks in thermoacoustic prime movers. Two series of experiments were conducted. One series was conducted with an open quarter wavelength resonator while the other series made use of a sealed half wavelength resonator. The first series quickly tested many different wire mesh stacks. The two best performing stacks, constructed from bolting cloth 10 and bolting cloth 16, were then used in the second series where more detailed measurements were possible.

In the first series the stack position was fixed. The acoustic medium and mean pressure was determined by atmospheric conditions. Acoustic amplitude was the measure of performance. This apparatus was simple and quickly provided results.

The second series of experiments were performed in a sealed resonator with a moveable plunger. This allowed variations in acoustic medium, mean pressure, and stack position. Neon gas was used at mean pressures from 6 to 86 kPa. By moving the plunger, the distance between stack and pressure antinode varied from 3.9 to 18.9 cm. Mesh stacks produced acoustic pressure amplitudes (RMS) as high as 20.9% of mean gas pressure. Some distortion was measured in the waveform, so acoustic pressure amplitudes were measured using voltage RMS. Converting to the traditionally measured peak acoustic pressure amplitude, the RMS reading is multiplied by $\sqrt{2}$ yielding a value of 29.5%, which is extremely high. The efficiency of these wire mesh stacks showed approximately 30% improvement over the typical polyester spiral roll stack. The shortest plunger to stack distances provided the highest acoustic amplitudes and were the most efficient.

B. CONCLUSIONS

Simple, randomly oriented, wire mesh screen stacks are suitable substitutes for the tediously fabricated, traditional, spiral roll stacks. They are simple to build, can be exposed to high temperatures, and have geometric parameters which are relatively easy to vary.

Short plunger to stack distances provide the highest amplitude. These shorter distances move the heat exchangers and stack closer to the pressure antinode which is also the velocity node; hence there is less velocity. Less viscous losses result, and an expected increase in amplitude and efficiency results.

Wire mesh efficiency is apparently much superior to the parallel plate geometry of the polyester spiral roll stack. In pin stack theory [Ref. 21 & 22] the parallel plate stack is reduced to a bundle of parallel wires oriented parallel to the flow. The pin stack capitalizes on the fact that the thermal penetration depth δ_κ, is larger than the viscous penetration depth δ_v. Although the wires of the mesh stack are oriented perpendicular to the oscillating flow, this same principle may account for the obvious improvement in efficiency.

The verdict on the best mesh hole size is not yet decided, but significant evidence was uncovered. The finer wire of bolting cloth is preferred over the standard grade wire size. Hole sizes 3 to 4 times that of the parallel plate gap were best. Parallel plate gaps are typically 3 to 5 times the thermal penetration depth. It may be proven subsequently that even larger hole size is better, as this experimental data did not bracket the optimum. The stack porosity is a significant variable in stack performance. Higher porosity meshes were the best. The highest and best porosity measured was 92.1%.

More specifically, a near term project of a thermoacoustically driven thermoacoustic refrigerator (TADTAR) was mentioned in Chapter I. The above results can be applied. The computer model utilized a parallel plate prime mover stack having a plate separation of 0.0108 inches. Applying a mesh conversion factor of 3.5 to this parallel plate separation gives the recommended mesh size.

$$\frac{1}{3.5(0.0108)} \approx 26 \text{ mesh.} \tag{4-1}$$

Thus a stack made from bolting cloth 26 should work as an initial try, although more open meshes may prove to be somewhat better.

C. RECOMMENDATIONS

The open prime mover was perfect for the simple experiments conducted in series one. The sealed prime mover is an excellent stack testing apparatus, but some improvements could be made. The thermal heat flow resistance in and between the heat exchanger components caused a significant variability in the temperature ratio. Improved heat exchangers would undoubtedly help minimize the heat flow resistance and stabilize the temperature ratio. A new simplified thermocouple feed-through design would significantly reduce assembly time. An improved temperature controller is also recommended.

Regarding future stack testing, several exciting ideas come to mind. Repeating the same experiments with more open mesh stacks should determine an optimum hole sizing. Meshes should be tried in thermoacoustic refrigeration experiments where the thermal penetration depths are much smaller. Sealed prime mover measurements using spacers between mesh screens should be performed. This minimizes the amount of material in the stack improving acoustic amplitudes and overall efficiency. Mesh screens of various hole sizes could be combined to match the variation in thermal penetration depths along the axis of the stack. Finally, a simple but crudely constructed pin stack geometry with the meshes oriented longitudinally should be tried.

LIST OF REFERENCES

1. Rott, Nikolaus, "Thermoacoustics," *Advances in Applied Mechanics*, v. 20, p.135 (Academic Press, Inc.,1980).

2. Swift, Greg W., "Thermoacoustic engines," Journal of the Acoustical Society of America, v. 84, p. 1145, 1988.

3. L. D. Landau and E. M. Lifshitz, *Fluid Mechanics* (Pergamon, Oxford, 1982).

4. Reference 2, Eq. 90.

5. Adeff, Jay A., "Measurement of a Space Thermoacoustic Refrigerator Performance," Master's Thesis, Naval Postgraduate School, Monterey, California, September 1990. app. C.

6. Reference 5, pp. 75-83.

7. Reference 5, pp. 70-75.

8. Condenser microphone, model 4133, serial number 1832470, Bruel & Kjaer, Decatur, GA.

9. Digitizing oscilloscope, model TDS 420, serial number B022912, Tektronics Inc., Beaverton, OR.

10. Digital multimeter, model 3478A, serial number 2911A59877, Hewlett-Packard Company, Loveland Instrument Division, P.O. Box 301, Loveland, CO 80537.

11. Piston phone, model 4228, serial number 1681325, Bruel & Kjaer, Decatur, GA.

12. Castro, Nelson C., "Experimental Heat Exchanger Performance in a Thermoacoustic Prime Mover," Master's Thesis, Naval Postgraduate School, Monterey, California, December 1993.

13. Piezoresistive pressure transducer, model 8530C-15, ENDEVCO, serial number L54E, 30700 Rancho Viejo Road, San Juan Capistrano, CA 92675.

14. System scanning thermometer, model 740, serial number 477078, Keithley Instruments Inc., Instrument Division, Cleveland, OH.

15. Miniature microprocessor temperature controller, model CN9000, Omega Engineering Inc., One Omega Drive, Box 4047, Stamford, CT 06907-0047.

16. Power supply amplifier, model 5530, serial number 054491, Techron Division of Crown International Inc., Elkhart, IN 46517.

17. Barometer, model UZ004, part of model 4228 pistonphone apparatus, serial number 1681325, Bruel & Kjaer, Decatur, GA.

18. Digital multimeter, model 3457A, serial number 2538A02272, Hewlett-Packard Company, Loveland Instrument Division, P.O. Box 301, Loveland, CO 80537.

19. Helium leak detector, model ASM 110 Turbo CL, serial number 797105-913, Alcatel Vacuum Products Inc.,40 Pond Park Road, South Shore Park Hingham, MA 02043.

20. I. Urieli and D. M. Berchowitz, *Stirling Cycle Engine Analysis* (Adam Hilger Ltd, printed in Great Britain by J W Arrowsmith Ltd, Bristol), p. 112.

21. Nesler, Scott F., "Comparison of a Pin Stack to a Conventional Stack in a Thermoacoustic Prime Mover," Master's Thesis, Naval Postgraduate School, Monterey, California, December 1994.

22. Gibson, Rodney J., "An Experimental Comparison of a Pin Stack in a Thermoacoustic Prime Mover," Master's Thesis, Naval Postgraduate School, Monterey, California, June 1996.

INITIAL DISTRIBUTION LIST

1.	Defense Technical Information Center 8725 John J. Kingman Rd., STE 0944 Ft. Belvoir, Virginia 22060-6218	2
2.	Dudley Knox Library Naval Postgraduate School Monterey, California 93943-5101	2
3.	Dr. Logan E. Hargrove ONR 331 Office of Naval Research 800 North Quincy Street Arlingto, VA 22217-5560	2
4.	Professor Thomas J. Hofler, Code PH/Hf Department of Physics Naval Postgraduate School Monterey, California 93943-5000	6
5.	Professor Anthony A. Atchley, Code PH/Ay Department of Physics Naval Postgraduate School Monterey, California 93943-5002	2
6.	Professor Robert Keolian, Code PH/Kn Department of Physics Naval Postgraduate School Monterey, California 93943-5002	1
7.	Professor William B. Colson, Code PH/Cw Department of Physics Naval Postgraduate School Monterey, California 93943-5002	1
8.	Professor Dan Holland, Code PH/Ho Department of Physics Naval Postgraduate School Monterey, California 93943-5002	1
9.	LCDR Mark S. Reed Physics Department U.S. Naval Academy Annapolis, MD 21402	2

INITIAL DISTRIBUTION LIST (continued)

10. Professor (retired) Robert D. Reed 1
50 Jumper Road
Shippensburg, PA 17257

11. Professor W. Patrick Arnott 1
Atmospheric Sciences Center
Desert Research Institute
P.O. Box 60220
Reno, NV 89506

12. Professor Henry E. Bass 1
Department of Physics and Astronomy
University of Mississippi
University, MS 38677

13. Professor Richard Raspet 1
Department of Physics and Astronomy
University of Mississippi
University, MS 38677

14. Dr. Gregory W. Swift 1
Los Alamos National Laboratory
MS K764
Los Alamos, NM 87545

15. Dr. David L. Gardner 1
Los Alamos National Laboratory
MS K764
Los Alamos, NM 87545

16. Professor Cila Herman 1
Department of Mechanical Engineering
G.W.C. Whiting School of Engineering
3400 N. Charles Street
Baltimore, MD 21218-2686

17. Professor Sameer I. Madanshetty 1
Department of Aerospace and Mechanical Engineering
Boston University, College of Engineering
110 Cummington Street
Boston, MA